HHS Public Access

Author manuscript

Cell Rep. Author manuscript; available in PMC 2023 October 23.

Published in final edited form as:

Cell Rep. 2023 April 25; 42(4): 112375. doi:10.1016/j.celrep.2023.112375.

Circadian protein TIMELESS regulates synaptic function and memory by modulating cAMP signaling

Estibaliz Barrio-Alonso[1], **Pablo J. Lituma**[1,7], **Michael J. Notaras**[1,7], **Robert Albero**[2], **Youcef Bouchekioua**[3], **Natalie Wayland**[1], **Isidora N. Stankovic**[1], **Tanya Jain**[4], **Sijia Gao**[3], **Diany Paola Calderon**[3], **Pablo E. Castillo**[5], **Dilek Colak**[1,6,8,*]

[1]Center for Neurogenetics, Feil Family Brain and Mind Research Institute, Weill Cornell Medical College, Cornell University, New York, NY, USA

[2]Institut d'Investigacions Biomè diques August Pi i Sunyer (IDIBAPS), Barcelona, Spain

[3]Department of Anesthesiology, Weill Cornell Medical College, New York, NY, USA

[4]Program of Neurosciences, Weill Graduate School of Medical Sciences of Cornell University, New York, NY, USA

[5]Dominick P. Purpura Department of Neuroscience, Albert Einstein College of Medicine, Bronx, NY, USA

[6]Gale & Ira Drukier Institute for Children's Health, Weill Cornell Medical College, Cornell University, New York, NY, USA

[7]These authors contributed equally

[8]Lead contact

SUMMARY

The regulation of neurons by circadian clock genes is thought to contribute to the maintenance of neuronal functions that ultimately underlie animal behavior. However, the impact of specific circadian genes on cellular and molecular mechanisms controlling synaptic plasticity and cognitive function remains elusive. Here, we show that the expression of the circadian protein TIMELESS displays circadian rhythmicity in the mammalian hippocampus. We identify TIMELESS as a chromatin-bound protein that targets synaptic-plasticity-related genes such as *phosphodiesterase 4B* (*Pde4b*). By promoting *Pde4b* transcription, TIMELESS negatively regulates cAMP signaling to modulate AMPA receptor GluA1 function and influence synaptic plasticity. Conditional

*Correspondence: dic2009@med.cornell.edu.

AUTHOR CONTRIBUTIONS

D.C. and E.B.-A. conceived the project, designed experiments, and wrote the manuscript with input from all authors. E.B.-A. performed molecular biology experiments and behavioral tests and executed the associated analyses. M.J.N. performed behavioral tests and ChIP-seq experiments. R.A. performed ChIP-seq analysis. P.J.L. performed electrophysiological experiments with input from P.E.C. P.J.L. helped write the manuscript. N.W., I.N.S., and T.J. helped with behavioral tests. Y.B. performed telemetry experiments with input from D.P.C. and S.G., and D.P.C. analyzed the telemetry data.

DECLARATION OF INTERESTS

The authors declare no competing interests.

SUPPLEMENTAL INFORMATION

Supplemental information can be found online at https://doi.org/10.1016/j.celrep.2023.112375.

deletion of *Timeless* in the adult forebrain impairs working and contextual fear memory in mice. These cognitive phenotypes were accompanied by attenuation of hippocampal Schaffer-collateral synapse long-term potentiation. Together, these data establish a neuron-specific function of mammalian TIMELESS by defining a mechanism that regulates synaptic plasticity and cognitive function.

In brief

Barrio-Alonso et al. examine mammalian TIMELESS function in synaptic plasticity and cognitive performance. They show that TIMELESS acts as a transcriptional regulator influencing PDE4B/cAMP levels that affect basal neurotransmission and, ultimately, memory. Neuronal deletion of *Timeless* impairs hippocampal long-term potentiation, as well as working and contextual fear memory in mice.

Graphical Abstract

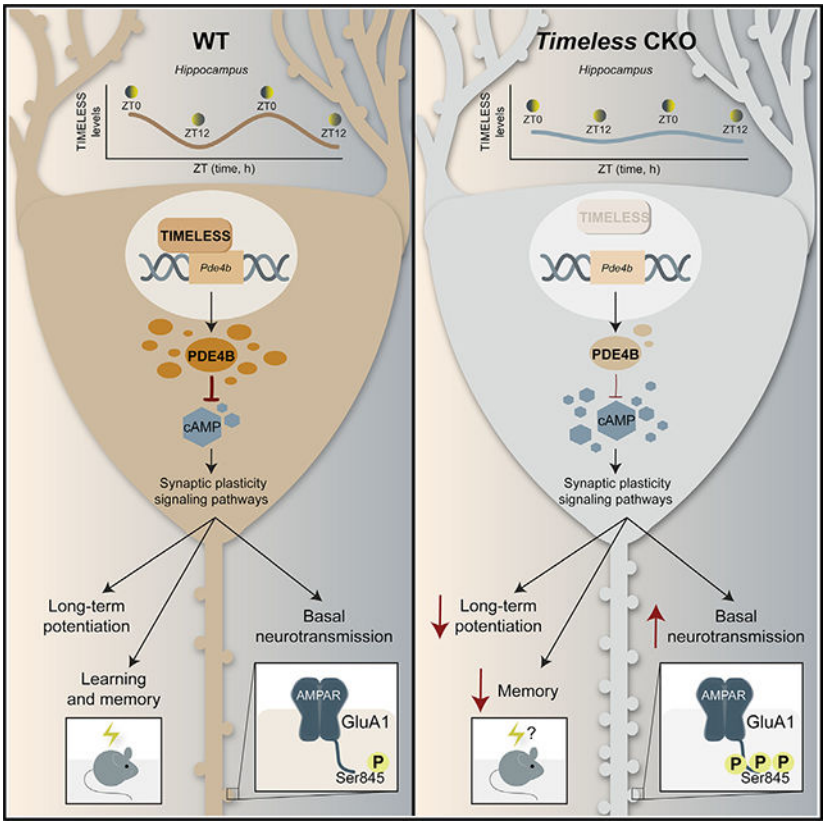

INTRODUCTION

Circadian rhythms are a set of physiological and behavioral patterns that enable most organisms to anticipate and adapt to environmental changes. The circadian clock affects crucial biological processes such as the cell cycle,[1] metabolism,[2] immunity,[3,4] aging,[5] and cognitive abilities.[6–8] In fact, growing evidence indicates that circadian rhythm disruption and memory impairments are closely linked.[9–12] Notably, recent findings

revealed that synaptic mRNAs display oscillatory rhythmicity[13] along with time-dependent phosphorylation of their synthesized proteins.[14] These reports suggest that circadian regulation of the synaptic transcriptome and phosphoproteome may exist. More importantly, these studies highlight that fine-tuned synchronization of molecular events during different phases of the day could support proper cognitive function. While other studies have identified that some circadian genes shape synaptic function and regulate memory in the hippocampus,[8,15] the precise molecular links between gene regulation, signaling cascades, neurotransmission, and animal behavior remain to be explored.

The first clock genes to be identified that control circadian rhythmicity were described in *Drosophila melanogaster*.[16,17] The *Drosophila* TIMELESS (dTIM) protein is part of a core clock feedback loop that, by dimerizing with PER1/2, causes tandem repression of BMAL1/CLOCK[18] to activate circadian clock-dependent genes. In mammals, mutations in *Timeless* and other circadian genes have been linked to cognitive disorders such as autism, schizophrenia, bipolar disorder, and Alzheimer's disease.[19–23] More specifically, in humans, *Timeless* mutations provoke cytoplasmatic accumulation, which destabilizes the interaction of PER2 and CRY2, resulting in familial advanced sleep phase (FASP) disorder.[24] Importantly, TIMELESS contains a DNA binding domain implicated in DNA damage repair[25–27] and is essential during embryonic development.[18,28,29] Altogether, these lines of evidence highlight the critical role of TIMELESS in gene regulation and disease. Yet, to date, the function of TIMELESS in cellular processes such as synaptic plasticity that can support cognition has not been revealed.

Here, we show that mammalian TIMELESS displays a region-specific pattern of expression in the adult mouse brain. Conditional deletion of the *Timeless* gene in adult excitatory neurons impaired working and contextual fear memory in mice. These memory phenotypes were accompanied by deficits in hippocampal synaptic plasticity in the form of long-term potentiation. We identified that TIMELESS promotes phosphodiesterase *Pde4b* transcription that in turn downregulates cAMP signaling in the hippocampus. Consistent with this regulatory function, *Timeless* deletion led to reduced PDE4B and increased cAMP levels associated with elevations in the AMPA receptor subunit GluA1 and GluA1-S845 phosphorylation. Morphological and functional assessment of Schaffer-collateral synapses showed an increase in both spine density and basal neurotransmission. Our findings provide evidence indicating that TIMELESS exerts transcriptional regulation to influence molecular signaling cascades that support synaptic plasticity and, ultimately, memory. Our study emphasizes the importance of circadian genes fine-tuning the dynamic range of synaptic plasticity in a temporal and region-specific manner to sustain proper brain function.

RESULTS

TIMELESS displays a circadian pattern of expression in the mouse brain

The expression pattern of TIMELESS in cortical and subcortical regions in mammals remains unclear. To determine the protein expression levels of TIMELESS in cortex and hippocampus, we performed immunohistochemistry in wild-type (WT) mouse brain. We found that TIMELESS is expressed in all cortical layers and the hippocampus at postnatal day >50 (Figure 1A). Notably, 96% of TIMELESS-positive cells co-localized

with the neuronal and excitatory markers NeuN and CaMKIIα, respectively (Figure S1). Recent studies showed that gene transcription and translation exhibit circadian rhythmicity that could regulate neuronal activity and connectivity in a region-specific manner.[13,14] Given the role of TIMELESS in supporting circadian rhythms in *D. melanogaster*[16,30,31] and mammals,[32–34] we sought to assess the circadian profile of TIMELESS protein. To do this, we maintained mice under a 12-h light and 12-h dark cycle (12:12 L/D) and collected tissue every 6 h, starting at light onset (zeitgeber time 0, ZT0). Similar to circadian proteins BMAL1, PER1/2, and CRY1/2/3,[10,12,15,18,35–37] TIMELESS protein levels displayed circadian rhythmicity in hypothalamus, cortex, and hippocampus (Figure 1B and Table S1). As previously reported, TIMELESS showed a substantial peak at ZT12 in the hypothalamus (Figure 1B and Table S1).[33,34] Intriguingly, while TIMELESS protein exhibited positive fluctuations in cortex and hypothalamus, we observed a downregulation in hippocampus (Figure 1B and Table S1). Taken together, our data indicate that TIMELESS displays region-specific circadian patterns of expression in the adult mouse brain.

Conditional deletion of *Timeless* disrupts hippocampal-dependent memory in adult mice

The circadian downregulation of TIMELESS in hippocampus relative to other brain areas raised the possibility that neuronal functions could be differentially controlled in this region. To address the role of TIMELESS in hippocampal function, we genetically ablated *Timeless* in excitatory neurons using a conditional knockout mouse for *Timeless* (*Timeless*$^{fl/fl}$) (Figure 2A). To target excitatory neurons, we used a Cre line in which Cre expression was driven by *CaMKIIα*, a robust promoter in the hippocampus. Since TIMELESS is required for embryonic development,[29] we controlled the spatiotemporal deletion of TIMELESS by crossing *Timeless*$^{fl/fl}$ mice with the tamoxifen-inducible Cre transgenic mouse (*CaMKIIα*:*CreER*^{T2}). *Timeless*$^{fl/fl}$; *CaMKIIα*:*CreER*^{T2} (CKO) offspring were treated with tamoxifen at postnatal day 42 to selectively delete *Timeless* in excitatory neurons of the adult forebrain. *Timeless*$^{wt/wt}$; *CaMKIIα*:*CreER*^{T2} offspring treated with tamoxifen were used as control (CTRL) (Figure 2A). Thus, this experimental design ensures that any potential phenotype would not be a result of non-specific Cre effects at cryptic *LoxP* sites. Two weeks post-tamoxifen treatment, a 53% reduction in *Timeless* mRNA expression and 32% decrease in TIMELESS protein in CKO mice were detected at ZT12 (Figures S2C and S2D). Meanwhile at ZT0, the deletion rate was significant but reached only >20% in mRNA and protein (Figures S2A and S2B). Given that both mRNA and TIMELESS protein shift expression levels in the light and dark periods in the hippocampus (Figure S3), our findings are in line with recent evidence highlighting the oscillatory nature of circadian gene expression[13,38] and raise awareness to dosing and sample collection throughout the circadian cycle. Hence, we focused our mechanistic assays at ZT12, when *Timeless* deletion is most robust.

Global ablation of circadian proteins leads to arrhythmic mice that exhibit alterations in the sleep-wake cycle.[30,39,40] Prior to initiating behavioral assays, we evaluated sleep-wake activity in CTRL and CKO mice. We assessed non-REM, REM, and awake states over a 5-day period in both groups. CKO mice exhibited no phase-shift differences relative to CTRL (Figure 2B). In addition, *Timeless* mRNA levels in hypothalamus of CKO animals remained unchanged (Figure S4). Together, these results suggest that our deletion

strategy mainly targeted the forebrain and did not impair a circadian rhythm driven by the hypothalamic suprachiasmatic nucleus (SCN).[15,41] However, we cannot exclude the possibility that *Timeless* deletion also took place in some other brain areas with an active *CaMKIIα* promoter that were not considered here. We detected no differences in weight and locomotor activity between CTRL and CKO groups (Figures S5A–S5C). Similarly, no anxiety-related behavior phenotypes were observed in *Timeless* CKO mice compared with CTRL mice (Figures S5D–S5G). Altogether, these data suggest that ambulatory activity or anxiety-related behavior are not confounding factors in the interpretation of other behavioral results.

We next sought to examine distinct aspects of memory function in *Timeless* CKO mice by using complementary behavioral assays. To assess short-term working memory and fear memory, we used the Y-maze[42] and contextual fear conditioning (CFC) tests,[42] respectively. In the Y maze, mice were exposed to two of three arms of the maze for 10 min. After 1 h, the mice were returned to the maze and were free to explore all three arms of the maze for 10 min. Preference for exploring the previously blocked arm, now the “novel” arm relative to the other arms, was quantified as an index of short-term working memory. Compared with CTRL mice, CKO animals exhibited a substantial decrease in preference for the novel arm vs. the familiar arms on the Y maze (Figure 2C). Exploration distances were similar between CKO and CTRL mice (Figure 2D), indicating that the decrease in novel arm preference in CKO mice could not be explained by differences in exploratory drive. Thus, in comparison with CTRL mice, CKO mice exhibited impaired short-term working memory.

We further subjected CTRL and CKO mice to the CFC test. In this behavioral paradigm mice are trained to become fearful of a conditioned stimulus (CS; in this case a neutral tone) by pairing it repetitively with an unconditioned stimulus (US; a mild [1 s/0.9 mA] foot shock). As the CS (tone) and US (shock) co-occur, mice become fearful of the CS and instinctively freeze. On day 1, we examined fear acquisition by scoring freezing behavior across five CS-US presentations. Mice were then exposed to the same context (the chamber) on day 2 without the CS. On this trial day, freezing behavior was interpreted as a measure of contextual fear memory, with more freezing indicating higher contextual fear. On day 3, the mice were exposed to the CS but in a different context. We again scored freezing, but this time interpreted it as an index of cued fear memory. Our results showed that tone-shock pairings elicited similar responses in CTRL and CKO animals (Figure 2E). However, *Timeless* CKO mice showed reduced freezing behavior when re-exposed to the fear context (Figures 2F and S6A) and the tone test phase (Figures 2G and S6B) compared with CTRL. To determine the potential contribution of *Timeless* to short-term fear memory, we examined contextual and cued fear responses 60 min after training. We observed no differences in freezing behavior between CTRL and CKO animals (Figures S6C–S6E), suggesting that *Timeless* contributes to long-term fear memory at ZT12. To evaluate the influence of the circadian cycle on long-term fear memory, we tested our animal cohorts at ZT0. In contrast to ZT12, we detected no fear memory deficits at ZT0 (Figure S7). Therefore, we proceeded to focus our experiments at time-point ZT12, when TIMELESS seems to have a more significant impact. Altogether, our experiments revealed that TIMELESS downregulation led to impairments in different forms of memory at specific periods of the circadian cycle.

Timeless deficiency attenuates long-term potentiation and elevates basal neurotransmission in hippocampus

Since memory deficits are often associated with altered synaptic plasticity, we next sought to assess long-term potentiation (LTP), a mechanism that elicits persistent changes in synaptic strength and is considered to support learning and memory.[43–45] To determine whether *Timeless* deletion impairs LTP, we performed electrophysiological recordings in acute hippocampal slices from CTRL and CKO mice (Figure 3A). Field excitatory post-synaptic potentials (fEPSPs) of Schaffer-collateral synapses were recorded for a 15-min baseline period in the presence of $GABA_A$ and $GABA_B$ antagonists ($GABA_A$, 100 μM picrotoxin; $GABA_B$, 3 μM CGP55845). Following the baseline period, LTP was elicited by theta-burst stimulation and fEPSPs were registered for 60 min post-induction. Quantification of fEPSP slope during the last 10 min of recordings revealed a significant LTP reduction in CKO animals compared with CTRL (Figure 3C). In addition, evaluation of synaptic strength determined by input-output analysis of Schaffer-collateral fEPSPs indicated a significant elevation in the CKO condition (Figure 3D). Meanwhile, paired-pulse ratio analysis across varying interstimulus intervals did not reveal any differences in presynaptic release (Figure 3E), thereby ruling out defects in presynaptic function. Elevation of basal neurotransmission can lead to altered LTP by limiting the induction of further synaptic potentiation, as previously described.[46,47] Altogether, our findings indicate that TIMELESS influences basal neurotransmission that affects synaptic plasticity in the hippocampus.

ChIP-seq identifies TIMELESS as a potential transcription activator of hippocampal synaptic plasticity pathways

To determine potential molecular pathways that could modulate basal neurotransmission via TIMELESS, we performed chromatin immunoprecipitation-sequencing (ChIP-seq) analysis. Given that TIMELESS protein contains a conserved DNA binding domain,[32,48,49] and clock gene products are well known to regulate transcription,[50] we explored the role of TIMELESS as a chromatin-bound transcriptional regulator. Using a validated TIMELESS antibody in hippocampal tissue from adult WT mice, we detected more than a thousand coding and non-coding regions bound by TIMELESS (Figure 4). Intriguingly, genomic annotation of proximal TIMELESS gene target readouts as peaks using the GREAT (Genomic Regions Enrichment of Annotations Tool) algorithm identified pathways exclusive to neuronal and synaptic functions (Figure S8). In addition, ingenuity pathway analysis (IPA) detected G-protein-coupled receptor pathways and canonical synaptic plasticity cascades as the most significant −log p values (Figure 4A). To assess the relevance of TIMELESS genomic targets, we overlapped the identified peaks with a subset of *bona fide* hippocampal active enhancers and promoters defined by high levels of the histone modification site H3K27ac.[51] In doing so, we revealed candidate genes related to synaptic functions (Table S1). Notably, we identified seven candidates directly bound by TIMELESS that strictly overlapped with active enhancers (Figure 4B). Thus, our findings point toward a role for TIMELESS as a DNA-bound transcriptional regulator of synaptic plasticity pathways.

TIMELESS positively regulates *Pde4b* expression that modulates cAMP levels and synaptic function in hippocampus

One of the most prominent TIMELESS candidate peaks was detected at the enhancer region of *Phosphodiesterase-4b* (*Pde4b*) (Figure 4C). Phosphodiesterases (PDEs) are an extended family of enzymes that inactivate cyclic nucleotide second messengers such as cAMP, which can influence cognitive function.[52,53] Previously, hippocampal cAMP was shown to fluctuate throughout the circadian cycle,[54] raising the possibility that PDEs could oscillate as well. Indeed, *Pde4b* mRNA and PDE4B protein levels displayed differences at ZT0 and ZT12 in hippocampi of CTRL mice (Figure S9). To determine whether TIMELESS regulates PDE4B and thereby cAMP, we measured their levels in hippocampal tissue obtained from CTRL and CKO animals. Quantification of *Pde4b* mRNA and PDE4B protein revealed a significant decrease in CKO animals in comparison with CTRL at ZT12 (Figure 5A). Reduction in PDE4B protein levels suggested that cAMP degradation could be impaired in *Timeless* CKO mice. Supporting this hypothesis, cAMP levels were significantly increased in CKO samples compared with CTRL (Figure 5B). Together, our data indicate that TIMELESS deficiency alters the PDE4B/cAMP signaling cascade.

In hippocampus, cAMP is a critical regulator of synaptic dynamics, learning, and memory.[54,57] To evaluate the effect of *Timeless* deletion and subsequent PDE4B/cAMP dysregulation on hippocampal synaptic transmission, we combined electrophysiology with selective pharmacology. While recording Schaffer-collateral fEPSPs we bath-applied forskolin (FSK; 50 μM, 15 min), an adenylate cyclase (AC) activator that recruits cAMP (Figure 5C). Following FSK treatment, we observed a modest potentiation in neurotransmission in the CKO condition (Figures 5D and 5E). In contrast, CTRL slices showed a transient suppression in neurotransmission (Figures 5D and 5E). Hydrolyzation of cAMP by PDEs to adenosine monophosphate (AMP) can lead to adenosine accumulation via 5′-nucleotidase.[55,56] In Schaffer-collateral and hippocampal mossy fiber synapses, adenosine activity can target presynaptic adenosine 1 receptors to transiently suppress transmitter release following cAMP activation.[58,59] Hence, the absence of suppressed neurotransmission in the CKO condition is consistent with reduced cAMP hydrolyzation and low adenosine production (Figure 5C). The reduction in PDE4B protein seen in CKO hippocampus tissue is the most plausible explanation for our finding.

To promote chemical potentiation of Schaffer-collateral synapses, we designed an FSK cocktail that contained nominal magnesium and the adenosine 1 receptor antagonist DPCPX at 100 nM. Under this condition, we observed a robust chemical potentiation in CTRL slices (Figures 5F and 5G). In contrast, CKO slices exhibited a significant reduction in chemical potentiation compared with CTRL (Figures 5F and 5G). These two pharmacological treatments indicated a dysregulation in cAMP signaling that could influence neurotransmission when TIMELESS protein is depleted.

Timeless deletion alters AMPA receptor function and spine densities in hippocampus

Functionally, AMPA receptors (AMPARs) mediate the vast majority of excitatory synaptic transmission by ensuring rapid responses to glutamate, the principal excitatory neurotransmitter in the mammalian central nervous system. Modulation of AMPAR activity

plays a crucial role in synaptic strength as well as learning and memory.[60–64] Of note, cAMP activation of protein kinase A (PKA) mediates phosphorylation of the AMPAR subunit GluA1 at serine 845 (S845), which increases the probability of open channels[65–68] and facilitates AMPAR insertion.[69,70] Thus, altered regulation of GluA1 might account for the elevated basal neurotransmission and memory phenotypes observed in *Timeless* CKO mice.

To investigate the impact of *Timeless* deletion on GluA1, we determined total GluA1 and GluA1-S845 phosphorylation levels in hippocampal tissue collected from CKO and CTRL mice. Quantification of *GluA1* mRNA levels revealed a more than 4-fold increase in CKO mice compared with CTRL (Figure 6A). Consistent with *GluA1* mRNA upregulation, *Timeless* CKO mice exhibited increased levels of GluA1 protein and enhanced phosphorylation of GluA1-S845 in western blot analysis (Figure 6B). Our molecular observations prompted us to interrogate AMPAR transmission of Schaffer-collateral synapses. Whole-cell patch-clamp recordings of CA1 pyramidal neurons enabled the measurement of AMPAR-mediated excitatory post-synaptic currents (EPSCs) and NMDA receptor (NMDAR)-mediated EPSCs to determine the AMPAR/NMDAR ratio in CKO and CTRL mice. Quantification of the AMPAR/NMDAR ratio revealed a significant increase in the CKO group compared with CTRL (Figure 6C), further supporting the elevation of basal neurotransmission in CKO mice.

Given that the majority of excitatory synaptic transmission in the brain occurs at dendritic spines,[74] we also quantified spine densities in the hippocampus of *Timeless* CKO animals. To label dendrites and spines, we delivered AAV-*CaMKIIα.GFP-Cre* virus to the dorsal CA1 by performing stereotaxic surgeries in both groups. Two weeks post-surgery, we imaged CA1 pyramidal neurons using confocal microscopy (Figure 6D). After acquiring maximum-intensity projections, we quantified dendritic spines along a 20-μm dendritic segment at least 20 μm away from the soma. Strikingly, we observed a significant increase in spine density in CKO dendrites compared with CTRL (Figure 6D). Taken together, these molecular, functional, and morphological findings indicate that TIMELESS plays a pivotal role in regulating the cAMP signaling pathway that influences synaptic function and structural plasticity (Figure 6E). Our findings strongly suggest that enhanced AMPAR activity and subsequent elevated basal neurotransmission could underlie the memory and synaptic plasticity deficits observed in *Timeless* CKO animals.

PDE4B supplementation rescues fear memory and spine density phenotypes by modulating cAMP levels in *Timeless* CKO mice

Last, we aimed to establish whether restoring PDE4B levels could rescue the structural and memory phenotypes observed in *Timeless* CKO mice. To restore PDE4B levels in the CKO hippocampus, we injected AAVDJ.hSyn1.mPDE4B6-T2A-mCherry concomitant with AAV9.*CaMKIIα*.GFP-CRE virus into CA1 to selectively supplement PDE4B in excitatory neurons that carried *Timeless* deletion (CKO + PDE4B) (Figures 7A and 7B). We also included an additional control group by injecting AAVDJ.hSyn1.mPDE4B6-T2A-mCherry into CTRL mice (CTRL + PDE4B) (Figures 7A and 7B). First, we determined whether PDE4B supplementation rescues cAMP and spine density phenotypes in *Timeless* CKO mice. CKO + PDE4B mice exhibited a significant reduction in hippocampal

cAMP levels compared with CKO (Figure 7C). Importantly, CTRL cAMP levels were not significantly different from the CKO + PDE4B condition (Figure 7C), indicating that PDE4B supplementation normalized cAMP to basal levels. Similarly, supplementing PDE4B in *Timeless* CKO mice prevented the increase in spine density observed in this group (Figure 7D).

Furthermore, we assessed the effect of PDE4B supplementation on the cognitive performance of CKO mice. As previously observed in Figure 2, *Timeless* CKO mice displayed attenuated fear memory compared with CTRL mice in the CFC test. In contrast, CKO mice supplemented with PDE4B (CKO + PDE4B) performed similar to the CTRL group, indicating a recovery in both contextual and cued fear memory (Figures 7F and 7G). During training, all four groups exhibited similar freezing percentage by the last tone-shock pairing (CS-US) (Figure 7E). However, CTRL mice supplemented with PDE4B showed reduced freezing percentage during the second tone-shock presentation (Figure 7E). Similarly, CTRL + PDE4B animals displayed low freezing behavior during the context phase compared with the CTRL group (Figure 7F). These findings suggest that elevation of PDE4B activity in CA1 may result in a minor learning delay and alters contextual memory in CTRL animals. Nevertheless, our behavioral assessments showed that selective PDE4B supplementation of excitatory hippocampal neurons was sufficient to restore fear memory function in *Timeless* CKO mice.

In conclusion, the results from these rescue experiments established that reduced PDE4B levels are responsible for fear memory and structural plasticity phenotypes observed in *Timeless* CKO mice. Collectively, our experiments indicate that TIMELESS protein regulates memory in the hippocampus by modulating the PDE4B/cAMP signaling hub that can influence synapse structure and function.

DISCUSSION

Here, we show a neuron-specific role of the circadian protein TIMELESS in synaptic and memory function of the mammalian brain. Our results reveal that TIMELESS, acting as a transcriptional activator, can balance PDE4B/cAMP levels to sustain adequate basal neurotransmission that affects synaptic plasticity and, ultimately, memory.

We found that TIMELESS expression displays circadian rhythmicity in hypothalamus, cortex, and hippocampus. Specifically, we observed that TIMELESS expression followed an anti-phase circadian pattern in hippocampus (Figure 1B). The distinct hippocampal expression of TIMELESS suggests that circadian proteins may control region-specific signaling mechanisms that influence neuronal circuit functions.[15,75–77] In support of this possibility, we detected dysregulated PDE4B/cAMP levels and impaired memory as *Timeless* CKO mice transitioned to the dark period (ZT12). Given that mice are nocturnal animals that display more active behaviors during the dark period, modulating hippocampal PDE4B/cAMP levels that influence synaptic plasticity and memory at specific periods of the circadian cycle is critical. Although the role of TIMELESS in clock gene regulation in the SCN remains unclear,[24,29,32,78–81] our study highlights that TIMELESS could regulate a wide array of cellular and molecular mechanisms. Of note, hippocampal ChIP-seq analysis

associated TIMELESS with G-protein signaling, cAMP response element-binding protein (CREB) activation, synaptic plasticity, and neuropathic pain. Together, our results are consistent with the notion that circadian proteins participate in neurobiological processes beyond circadian rhythm generation. Further research is required to address the functional impact of the distinct TIMELESS expression profiles seen in different brain areas.

In our study, TIMELESS deficiency in CaMKIIα-positive excitatory neurons led to impairments in different forms of memory. Because the sleep cycle is a circadian rhythm driven by SCN activity, whose disruption can abrogate memory maintenance,[82,83] ensuring that *Timeless* deletion did not alter the sleep cycle was crucial for the interpretation of our behavioral results. Since sleep-wake activity in CKO animals was not disturbed (Figure 2B) and hypothalamic *Timeless* mRNA levels in CKO and CTRL animals were comparable (Figure S4), *Timeless* deletion appears to primarily target excitatory neurons of the forebrain. However, we cannot exclude the possibility that *Timeless* ablation took place in CaMKIIα-positive excitatory neurons outside this specific brain area. TIMELESS deficiency led to impairments in contextual and cued fear memory assessed by CFC (Figures 2F and 2G). Similarly, the Y maze revealed alterations in short-term working memory in CKO animals (Figure 2C). Our observations indicate that TIMELESS regulates different forms of memory but not fear acquisition. The selective effect of TIMELESS on memory suggests that circadian proteins may contribute to cellular and molecular mechanisms that influence the recruitment of specific neural ensembles to maintain signal to noise during learning and memory processes. Indeed, our findings are in line with previous research that identified a link between circadian rhythms and distinct forms of memory.[15,41,75,76] Furthermore, memory formation has been shown to temporally rely on cAMP, mitogen-activated protein kinase (MAPK), and CREB, which display circadian rhythmicity in the hippocampus.[54,84] Intriguingly, activation of the transcription factor CREB was associated with TIMELESS in our ChIP-seq analysis. Investigating the outcome of CREB activation by TIMELESS may uncover underappreciated circadian-mediated regulatory pathways involved in mammalian learning and memory.

Based on phylogenetic analysis, mammalian TIMELESS has higher sequence homology to dTIM2 (TIMEOUT), which was shown to participate in DNA metabolism and maintenance of chromosomal integrity in *D. melanogaster*.[29,31,85] Similarly, our findings identified TIMELESS as a chromatin-bound protein that can exert transcriptional regulation. TIMELESS displayed a robust interaction with signaling pathways related to synaptic modulation in the adult mouse hippocampus (Figures 4A and 4B and Table S2). We identified that TIMELESS promotes the expression of PDE4B, a key PDE involved in hippocampus development and a critical regulator of cAMP.[52,53] PDE4B expression exhibited circadian fluctuation in the hippocampus (Figure S9), consistent with previously reported cAMP dynamics.[54] Accordingly, *Timeless* deletion led to reduced PDE4B levels and, consequently, an increase in cAMP concentration (Figures 5A and 5B). When activated by cAMP, PKA phosphorylates AMPAR-GluA1 at S845 to enhance GluA1 delivery to the extrasynaptic membrane, increase open-channel probability, and prevent surface scaling-down of AMPARs.[60,66,68,86–91] In agreement with these reports, elevated cAMP concentration was associated with an increase in GluA1-S845 phosphorylation and GluA1 expression in the CKO condition (Figure 6B). Considering that PKA enhances local protein

synthesis[92] and activates CREB to boost expression of synaptic plasticity-related genes,[93,94] such scenario may explain the increase in *GluA1* mRNA and protein seen in CKO mice (Figure 6A).

To evaluate the functional outcome of AMPAR upregulation, we measured the AMPAR/NMDAR ratio and synaptic strength of Schaffer-collateral synapses. Consistent with our molecular assays, we observed an increase in both of these synaptic properties in CKO mice (Figures 5C and 3D). Elevated basal neurotransmission could in part explain the impairment of LTP induced by theta-burst stimulation in CKO animals (Figures 3B and 3C). To promote potentiation, we implemented a chemical approach that elicited synaptic potentiation in the CKO condition (Figures 5F and 5G). However, in comparison with CTRL, the magnitude of CKO chemical potentiation remained significantly reduced (Figures 5F and 5G). Our observations suggest that enhanced cAMP signaling elevated basal neurotransmission that limited the dynamic range of synaptic plasticity. Thus, the ability of TIMELESS to regulate the expression of PDE4B and subsequently modulate cAMP levels may have an impact on LTP magnitude. In this regard, mounting evidence indicates that PDE4B plays a direct role in LTP: early LTP may be controlled by PDE4B via indirect PKA activation, and late LTP can be modified by PDE4B through its influence on CREB.[95–98] Importantly, our findings highlight that circadian proteins may fine-tune molecular signaling mechanisms underlying synaptic plasticity.

We observed that accentuated cAMP signaling and elevated AMPAR activity were associated with memory impairments upon disruption of TIMELESS in excitatory neurons of the adult mouse forebrain. In contrast, previous studies have shown that increased cAMP signaling enhanced cognitive processes.[95,99,100] A potential explanation for this disparity is the duration and method of cAMP upregulation. By supplementing PDE4B we restored cAMP to normal levels and observed a recovery in memory function (Figures 7C and 7E–7G). Our findings imply that temporal manipulation of cAMP signaling by inducing or reducing PDE4B levels may result in different memory phenotypes. Similarly, the decrease in different PDEs can improve or impair memory in a task-dependent manner.[95,71,101] Hence, *Timeless* downregulation could trigger chronic cAMP activity that may have unexpected effects on memory function. In this regard, we found a distinct pattern of PDE4B expression but no memory deficits at ZT0 (Figures S7 and S10). Our findings emphasize the impact of the circadian cycle on memory performance and transcription-translation regulation.[14,15,102,103]We also cannot exclude the possibility that, in addition to the cAMP cascade, PDE4B regulates other signaling pathways supporting cognitive function.[53]

Along with alterations in memory and cAMP activity, we also detected changes in dendritic spine structure in CKO mice. Spine density most likely operates in an optimal range to subserve proper cognitive function; thus, too many or too few spines is deleterious.[104,105] There is strong evidence that spine formation exhibits circadian regulation,[106] and CA1 pyramidal neurons possess higher spine density during the active phase than in the passive period.[107] Moreover, the influence of circadian genes on microanatomy and structural plasticity across phyla has been previously reported in the nervous system of the fly and cockroach.[108–110] In our studies, reductions in TIMELESS resulted in enhanced spine

densities of CA1 pyramidal neurons (Figure 6D). PDE4B supplementation in CKO animals restored spine density and memory (Figures 7D–7G). Although our findings suggest that TIMELESS exerts circadian control of neuronal morphology to support cognitive functions by modulating PDE4B/cAMP signaling, we cannot exclude the possibility that other genes/signaling pathways are involved in this regulation. In fact, ChIP-seq analysis identified genes related to spine structure that could be regulated by TIMELESS. These candidate genes include *Shank2*, *Myosin V*, *Disc1*, *Cdc42*, and *Rhob* (Table S2). Future work should explore the effects of these factors on synaptic modulation and memory. Nevertheless, our results indicate that circadian protein regulation of signaling cascades and gene expression may support modifications to synapse structure.

In summary, our study revealed the distinct protein expression pattern of TIMELESS in the mammalian brain throughout the circadian cycle. Specifically, we observed an attenuation of TIMELESS protein in the hippocampus as mice transitioned to the dark period (ZT12) (Figure S3). At this time point, we detected an elevation in PD4EB protein (Figure S9), consistent with cAMP downregulation in the hippocampus at ZT12.[54] Because TIMELESS acts as a transcriptional regulator of *Pd4Eb* (Figures 4, 5, and 7), it might contribute to synaptic plasticity and memory processes by mediating regulation of PD4Eb/cAMP levels at specific periods of the circadian cycle. However, we did not observe major differences in memory performance between ZT0 and ZT12 in CTRL mice (Figure S11). One possible explanation for our result is that differences in physiological events, including gene transcription and translation, epigenetic processes, cell signaling, synaptic excitability, structural plasticity, and hormone secretion, fluctuate[13,14,111] and may affect different aspects of behavioral performance across the circadian cycle. Nevertheless, downregulation of TIMELESS protein levels in CKO mice reduced PD4EB amplitude, which was associated with memory deficits at ZT12. In contrast, at ZT0, the memory deficits were no longer present when PD4EB amplitude significantly increased in CKO mice (Figures S7 and S10). This is consistent with our findings that memory phenotype is rescued in CKO at ZT12 following PD4EB supplementation. Our study highlights the complex and diverse effects that circadian proteins can elicit at specific time points of the light-dark cycle under normal or disruptive conditions in the mammalian brain.

Circadian gene mutations have been linked to cognitive disorders such as autism, schizophrenia, bipolar disorder, and Alzheimer's disease.[19–23,112–114] More precisely, single-nucleotide polymorphisms in the human *Timeless* gene have been detected in individuals diagnosed with bipolar disorder and schizophrenia.[21] Meanwhile, pharmacological suppression of PDEs has been linked to a variety of autism-like symptoms and cognitive disorders.[52,115,116] Given the essential role of TIMELESS in embryonic development[29,117] and its transcriptional influence on PDE4B, our study raises awareness of circadian proteins regulating synaptic plasticity and circuit formation in the developing nervous system. In light of our results, the potential contribution of *Timeless* mutations to PDE4B/cAMP dysregulation in neurological diseases merits investigation.

Limitations of the study

We identified TIMELESS as a transcriptional activator that can modulate synaptic plasticity and cognitive functions in part by regulating PDE4B/cAMP levels to maintain proper basal neurotransmission in the hippocampus. However, the extent to which TIMELESS influences other downstream cAMP-dependent signaling pathways and synaptic/structural plasticity was not examined. Similarly, we cannot exclude the possibility that some of the phenotypes observed in CKO mice are fully or partially caused by alterations of pathways other than PDE4B/cAMP signaling. Furthermore, studies have reported the impact of other circadian genes (e.g., BMAL1) on memory function; hence, we cannot discard their influence on TIMELESS activity or the activation of a compensatory mechanism(s) at later adult stages. Our findings suggest that TIMELESS function is time sensitive. However, our study focused on two circadian time points (ZT0 and ZT12); we did not explore the impact of TIMELESS across the diurnal cycle. In this regard, our ChIP analysis was performed on a single time point in the hippocampus. TIMELESS genomic interactions may vary in a circadian-and brain-region-specific manner. Assessment of TIMELESS's role in various brain regions throughout the light-dark cycle will provide further insight into the interplay of oscillatory physiological events in the brain.

STAR+METHODS

RESOURCE AVAILABILITY

Lead contact—Further information and request for resources and reagents should be directed to and will be fulfilled by the lead contact, Dilek Colak (dic2009@med.cornell.edu).

Materials availability—This study did not generate new unique reagents.

Data and code availability

- All data supporting the findings of this study are available from the corresponding author upon reasonable request. ChIP-seq data have been deposited at GEO and are publicly available as of the date of publication. Accession number is listed in the key resources table.
- This paper does not report original code.
- Any additional information required to reanalyze the data reported in this paper is available from the lead contact upon request.

EXPERIMENTAL MODEL AND SUBJECT DETAILS

Mice—Animal experiments were conducted in accordance with the ethical guidelines of the National Institutes of Health and approved by the Institutional Animal Care and Use Committee at Weill Cornell Medicine and Albert Einstein College of Medicine. All animals were under *ad libitum* conditions and were group housed with littermates. Mice were maintained on a 12 h light/dark (LD) schedule. Zeitgeber time (ZT) is determined from the animal's LD cycle, with lights-on designated as ZT0 and lights-off as ZT12. Our behavioral assays and experimental procedures were performed at ZT12, unless otherwise stated.

We genetically ablated *Timeless* in post-mitotic neurons using a conditional knockout mouse of *Timeless*, which carries flanked LoxP sites in the 14th exon of this gene (C57BL/6N-A<tm1Brd> *Timeless*<tm1a (EUCOMM) Hmgu>/Wtsi). Since *Timeless* is required for embryonic development, we temporally controlled *Timeless* ablation by crossing $Timeless^{fl/fl}$ with a mouse line that expresses tamoxifen-inducible Cre under the *CaMKIIα* promoter (*CaMKIIα*::$CreER^{T2}$).[118] Typically, we induced Cre in *Timeless* CKO mice ($Timeless^{fl/fl}$;*CaMKIIα*:$CreER^{T2}$,CKO) and control mice ($Timeless^{wt/wt}$; *CaMKIIα*:$CreER^{T2}$, CTRL) at 6 – 7 weeks old and performed analyses in young adults 2– 4 months old. Both male and female mice were used. For Cre induction, tamoxifen was prepared in corn oil at 40 mg/ml and was administered at 200 mg/kg intraperitoneally (IP) in 5 doses (the first 3 doses in consecutive days and the last 2 doses spaced by 1 or 2 days). Experiments were carried out at least 2 weeks after tamoxifen treatment.

METHOD DETAILS

Immunohistochemistry—Mice were transcardially perfused with 4% PFA (after PBS flush). Brains were fixed overnight, moved to 30% sucrose, and stored at 4 °C. Brains were embedded in OCT compound and frozen at −80 °C for coronal sectioning using a cryostat (30 μm or 300 μm). Slices were permeabilized in 1% Triton X for 30 min and blocked with 10% normal goat serum for 1 h. Primary antibodies were incubated overnight at 4 °C. The following day, secondary antibodies were added for 2 h at room temperature (RT). To visualize the nucleus of individual cells, Hoescht was applied in the final wash prior to mounting. Primary antibodies: TIMELESS (rabbit; Abcam, ab72458), NeuN (mouse; Millipore, MAB377), CaMKIIα (rabbit; Millipore, C265) and GFAP (chicken; Thermofisher, PA1–10004). Secondary antibodies: Alexa 488 (anti-rabbit; Thermofisher, A-11008) and 647 (anti-mouse; Thermofisher, A-21235 and anti-chicken; Thermofisher, A-21449).

Western blotting—Mice were sacrificed by cervical dislocation, brains were snap-frozen on dry ice and stored at −80 °C for downstream applications. The whole hippocampi, cortices, and hypothalamus were dissected and lysed using ice-cold RIPA buffer containing a protease inhibitor (Millipore, 539134) and phosphatase inhibitor cocktail (Sigma, P5726). Samples were kept on ice and sonicated briefly. The insoluble fraction was removed by centrifugation at 18,000 × g for 15 min at 4 °C. Protein concentration was determined using a BCA protein assay kit (Thermofisher, 23225). Protein was extracted from cortex, hippocampus and hypothalamus and aliquoted into samples of 60, 30 and 90 μg, respectively. After adding NuPAGE® LDS Sample Buffer (Thermofisher, NP0007) and NuPAGE® Sample Reducing Agent (Thermofisher, NP0009), samples were boiled for 10 min at 97°C and proteins were separated by electrophoresis on 7.5 % Bis-Tris SDS-gels (BioRad, 4561025). After transfer, the nitrocellulose membranes (BioRad, 1620212) were blocked for 2 h at room temperature with 5% milk or BSA in Tris-buffered saline (TBS) containing 0.1% Tween-20 (TBS-T) and then incubated overnight with primary antibodies at 4 °C. The following primary antibodies were used: anti-TIMELESS (rabbit; Abcam, ab50943), anti-Actin (mouse; Sigma, A5316), anti-PDE4B (rabbit; Abcam, ab170939), anti-GluA1 (rabbit; Millipore, 04–855), anti-GluA1 pS845 (rabbit; Millipore, AB5849). Blots were washed and incubated for 2 h in the same buffer containing secondary antibody at

RT. Blots were imaged using LI-COR Odyssey CLx imaging system and quantified using ImageStudioLite (LI-COR). All experiments were performed with a minimum of 3 technical replicates.

Quantitative RT-PCR—Total RNA from hippocampal lobes was isolated using a RNA extraction kit (Zymo, R2053), following the manufacturer's instructions. 500 ng of RNA was transcribed into cDNA using oligo (dT) and random primers using a cDNA synthesis Kit (Thermofisher, AB1453B). Quantitative Real-Time PCR (qRT-PCR) reactions were performed using the SsoAdvanced™ Universal SYBR® Green Supermix (BioRad, 1725270). For each reaction 10 ng cDNA was used. Primers used: *Timeless* (Fw: ATGAACTGTGAACTTCTAGCCAC; Rev: CCTCAGGTATCGGATCAAATCCT), *GluA1* (Fw: CTAGGCTGCCTGAACCTTTG; Rev: GGGAAGATTGAATGGAAGCA), *Pde4b* (Fw: GCGAGATGGCTTCAAACAA; Rev: CAGACACCTGGTTCCCTGAT), β-*Actin* (Fw: ATGGAGGGGAATACAGCCC; Rev: TTCTT TGCAGCTCCTTCGTT). All primer pair efficiencies were determined by qPCR of tenfold dilutions of cDNA samples and linear regression of Ct values in the range of Ct = 20–30. Upon confirmation of valid primers, the ΔΔCt method[119] was used for quantification of mRNA levels. Relative expression levels were normalized to β-*Actin* mRNA.

EEG/EMG wireless transmitter implantation—CKO mice (n = 3) and C57BL6 wild-type (n = 2) male mice were anesthetized in an induction chamber with isoflurane at a concentration of 4% by volume in O_2. Animals were then transferred to a stereotaxic frame and maintained under anesthesia using a nose cone with isoflurane at a concentration of 2% by volume in O_2. The concentration of isoflurane was monitored using a gas analyzer (Riken Fi-I gas analyzer). Body temperature was maintained at ~37 °C using a temperature regulator coupled to a rectal temperature probe (CWE Inc), and eyes were protected with ophthalmic ointment. A craniotomy was made (AP +1.0 mm, ML +1.0 mm, relative to bregma).

A subcutaneous pocket was created along the animal's dorsal flank using small blunt-tipped dissecting scissors by pushing aside connective tissue. Then, a 3.9 g transmitter (PhysioTel F20-EET, Data Sciences International (DSI), St Paul, MN, USA) was placed into the pocket ensuring biopotential leads were oriented cranially. The electroencephalogram (EEG) lead was placed in the craniotomy and secured with dental acrylic. The electromyogram (EMG) lead was threaded through the cervical trapezius muscle via a small incision made by a 20-G needle and held in place with non-absorbable suture. Animals received Flunixin 5 mg/Kg and were allowed to recover for 7 days.

After recovery from surgery, EEG and EMG recordings were acquired continuously for 5 days. Recordings took place in a designated room with minimal background disturbances. The room light strictly followed a 12:12h light/dark cycle, and the temperature and humidity were kept constant. During the 5-day recording period, animals were individually housed in standard plexiglass home cages on receiver plates (RPC1, DSI, MN). The latter sent the EEG and EMG waveform data via an exchange matrix (DSI, MN) to a computer installed with Ponemah V5 software from DSI at a sampling rate of 250 Hz.

Behavioral assays—To study the role of TIMELESS in learning and memory, we induced Cre expression in 6–8 weeks old *Timeless* CKO mice (CKO +/+, Cre +) by tamoxifen. Aged-matched mice from cohorts that were Cre+ but lacked the LoxP construction were also injected with tamoxifen and used as controls (CTRL). Experiments were performed a minimum of 2 weeks after the last tamoxifen dosing (2–3 months of age). For all behavioral assays, mice were habituated to the testing room for a minimum of 30 min, and testing was performed at the same time of day except where noted. Y-maze[42,120] was utilized as a measure of short-term spatial memory and the Fear Conditioning test[42,120] was used to examine fear memory. Briefly, the Y-Maze consists of exposing mice for 10 min to two of three arms of the maze as a training trial. The third arm, designated as the novel arm, was blocked during this first phase and was pseudorandomized between mice. 1 h after training, mice were returned to the maze and were able to freely explore all three arms for 5 min. Quantification of the time spent exploring the novel arm, relative to the other arms was our index of short-term spatial memory. This was calculated as the cumulative time (s) exploring the novel arm / average time exploring the familiar arms $\left(Preference\ index\ = \frac{Time\ in\ novel\ arm\ (s)}{Avg.\ time\ in\ familiar\ arm\ 1\ and\ 2}\right)$. Distance travelled was also recorded and analyzed as an additional metric of exploratory drive. Context and cue dependent fear conditioning is a paradigm that probes Pavlovian associative learning and fear memory. Mice are trained to become fearful of a tone as a conditioned stimulus (CS) in response to an aversive unconditioned stimulus (US, 1 second/0.9 mA mild electrical foot shock repeated 5 times). Mice display freezing behavior as a conditioned response (CR) and is recorded in all phases of testing as evidence of learning (day 1) and/or fear memory (days 2–3). On day 1, after mice were habituated in the cage for 2 min, each mouse was presented with 5 successive 30 s periods of an audible tone (CS) that co-terminated with a mild foot shock. Learning was evaluated by plotting % freezing to each successive tone presentation as a time-course. On day 2, mice were placed for 6 min in the same context but without any tone or shock to assess retrieval of the cage-shock association (context-dependent associative memory). On day 3, we assessed the ability of mice to retrieve the tone-shock association by placing animals in a novel context and administering only the CS. We reported freezing % as an average of all CS presentations on this day of testing. On all testing days, % freezing behavior was a readout for fear memory. All measurements were determined by automated software from Med Associates Inc. Other behavioral tests used to assess locomotor activity, anxiety-like behavior and repetitive behaviors were performed as previously described.[42] Mice tested at ZT12 and ZT0 were transferred from the housing room to the behavioral room. During transport, mice were protected from natural light. Upon arrival to the behavior room, mice were allowed to acclimate to the behavioral lighting conditions (75% red and 25% white light) for at least 1 h prior to initiating experiments.

Stereotaxic surgery and hippocampal spine density analysis—To measure hippocampal spine density, dorsal CA1 hippocampal neurons in CTRL and *Timeless* CKO mice were labeled with an adeno associated virus that expressed GFP under the control of the excitatory neuron promoter, *CaMKIIα (*AAV9-*CaMKIIα*.eGFP-CRE; Addgene, 105551-AAV9). For rescue experiments, CRE expressing virus and PDE4B virus, AAV-DJ(N589X).hSyn.xmPDE4B.IRES. mCherry.WPRE.SV40 (Penn Vector core) were

delivered in a 1:3 ratio. As previously described 42, 1–2 μl of the virus was injected bilaterally using a 10 μl nanofil syringe (World Precision Instruments) fitted with a 33-gauge beveled needle. The stereotaxic coordinates AP: −2, ML: 1.6, DV: 1.5-.25 were used to target the dorsal CA1. Meloxicam (2 mg/kg) was used as an analgesic and bupivacaine (Marcaine 0.25% solution) was applied as a local anesthetic. Eyes were protected with ophthalmic ointment and wounds were closed with tissue adhesive (Vetbond, 3M) as post-surgery treatment. Mice were transcardially perfused 14 days after surgery with 4% PFA. Brains were extracted and sectioned at 300 μm. Hippocampal dendrites were imaged on an Olympus FluoView-FV1000 confocal microscope using 63X (1.4 NA) zoom 4.5. From acquired images we generated maximum intensity projections from z-stacks using optical sections (0.25 μm per section). To quantify, we identified a 20 μm dendritic segment at least 20 μm away from the soma and counted individual spines in a blind manner using ImageJ.

Chromatin immunoprecipitation (ChIP)—ChIP assays were performed according to the protocol from the Merck Millipore Chromatin Immunoprecipitation Kit (EZ-ChIP Kit, #17–371; Merck Millipore).[11,15] Magna ChIP™ G Tissue Kit (#17–20000; Merck Millipore) was used for isolating the mouse hippocampal tissue, with minor modifications. In brief, tissue was dissociated and cross-linked with 1% formaldehyde for 5 min, quenched by adding glycine, washed, and lysed in the cell lysis buffer. Sonication of the dissolved pellet was performed on wet ice to shear chromatin to 200–1000 bp, and chromatin was immunoprecipitated overnight at 4°C with 1 μg of anti-TIMELESS (rabbit; Abcam, ab72458). Before immunoprecipitation, 10 μl of the lysates was saved as input for normalization purposes. As a negative control, anti-mouse IgG was used. Antibody/DNA complex was collected and then DNA was purified after washing and reverse-crosslinking treated with Protein K. ChIP-Seq was performed at WCM's Genomics Core facility. Reads were aligned against mouse genome (mm10) using Bowtie2 (v2.4) and samtools (v1.14). Peaks were assigned using MACS v2.1.1 and bigwigs were generated with Deeptools 2.0, both with default options. There were 3,430 high-confident peaks called after peak calling and IDR analysis. GOrilla was used to analyze gene ontology pathways and Ingenuity Pathway Analysis was performed using candidate genes overlapping promoters, TTS, exons and introns. Peaks were overlapped with a list of hippocampal enhancers in adult mice defined by the presence of H3K27ac published by Gjoneska et al, 2015. ChIP-Seq data might be found at GEO Accession (GSE208149).

Cyclic AMP ELISA measurement—Cyclic AMP (cAMP) content was measured using the enzyme-linked competitive immunoassay Cyclic AMP Complete ELISA kit (ENZO Life Sciences, #ADI-900–163) following the manufacturer's instructions. Briefly, dissected hippocampal tissue was flash frozen in dry ice and extracted in 0.1 M HCl. Only 1 hippocampal lobe was used for the assay and then diluted 1:25 to fit the standard curve. Data are expressed as pmol cAMP per mg of total protein after protein normalization of each sample.

Hippocampal slice preparation—Male and female mice >P50 were anesthetized with 4% Isoflurane followed by perfusion with 25 mL of cold NMDG solution containing in (mM): 93 NMDG, 2.5 KCl, 1.25 NaH_2PO_4, 30 $NaHCO_3$, 20 HEPES, 25 glucose, 5 sodium

ascorbate, 2 Thiourea, 3 sodium pyruvate, 10 $MgCl_2$, 0.5 $CaCl_2$, brought to pH 7.35 with HCl. After perfusion, the brain was extracted, and isolated hippocampi were cut using a VT1200s microslicer in cold NMDG solution. Acute hippocampal slices (300–400 μm) were collected and placed in a chamber containing extracellular artificial cerebrospinal fluid (ACSF) recording solution containing (in mM): 124 NaCl, 2.5 KCl, 26 $NaHCO_3$,1 NaH_2PO_4, 2.5 $CaCl_2$, 1.3 $MgSO_4$ and 10 glucose. The slice chamber was warmed in a water-bath at 33–34°C. After 10 min of completing slice collection, the chamber was moved to room temperature and slices were allowed to recover for at least 45 min prior to experimentation. All solutions were equilibrated with 95% O_2 and 5% CO_2 (pH 7.4).

Electrophysiology—Electrophysiological experiments were performed at 26.5 ± 1 °C (unless otherwise stated) in a submersion-type recording chamber perfused at 2 mL/min with ACSF supplemented with the $GABA_A$ receptor antagonist, picrotoxin (100 μM). Whole-cell patch-clamp recordings of CA1 pyramidal cells were obtained using patch-type pipette electrodes (3–4 MΩ) containing intracellular solution (in mM): 131 cesium gluconate, 8 NaCl, 1 $CaCl_2$, 10 EGTA, 10 glucose, 10 HEPES, pH 7.25 (280–285 mOsm). KOH was used to adjust pH. Series resistance (10–20 MΩ) was monitored throughout all experiments with a −5 mV, 80 ms voltage step, and cells that exhibited a series resistance change (>20%) were excluded from analysis. A stimulating glass electrode was filled with ACSF and placed in *stratum radiatum* to activate Schaffer collateral inputs every 10 s using a Isoflex stimulus isolator (A.M.P.I) with a 100 μs pulse width duration. AMPAR/NMDAR ratio was assessed by recording evoked AMPAR excitatory postsynaptic currents (EPSCs) at $V_h = -65$ mV and NMDAR-EPSCs at $V_h = +40$ mV in the presence of 10 μM NBQX.

Extracellular field excitatory postsynaptic potentials (fEPSPs) were recorded at 28 ± 1 °C using a patch-type pipette filled with 1 M NaCl. For long-term potentiation (LTP) recordings, slices of 400 μm thickness were stimulated every 20 s for a baseline fEPSP period of 15 min. LTP was induced by theta-burst stimulation (TBS) consisting of: 10 bursts of 5 pulses at 100 Hz delivered every 200 ms (interburst interval) repeated 4X (every 5 s) as previously described.[121] LTP experiments were carried out in the presence of picrotoxin (100 μM) and CGP-55845 (3 μM) to block inhibitory transmission. The last 10 min of fEPSP responses were compared to baseline averaged responses to determine the magnitude of potentiation. For extracellular field input-output experiments the Isoflex stimulator was increased from 0–15 μA in 2.5 μA increments. Slopes of fEPSP responses and amplitudes of fiber volleys were determined using Igor Pro 6. Origin Pro 9 software was used to calculate slopes of linear-fit curves for input-output functions. Paired-pulse ratio (PPR) was evaluated by delivering two stimuli at various inter-stimulus intervals (10–500 ms) and measuring the ratio of fEPSP slopes ($fEPSP_{slope2}/fEPSP_{slope1}$). Forskolin (FSK) pharmacology and chemical potentiation experiments were performed at 26.5 ± 1 °C in the presence of picrotoxin (100 μM). Schaffer-collateral inputs were stimulated every 10 s and fEPSP slopes were registered for a baseline period of 10 min. Following the baseline period, FSK (50 μM) was bath-applied for 15 min and fEPSP responses were collected for 30 min post-FSK treatment. To induce chemical potentiation a cocktail of FSK (50 μM), DPCPX (100 nM), and nonimal Mg^{+2} ACSF was bath-applied for 15 min and fEPSP responses were collected for 40 min post-FSK cocktail treatment. Whole-cell voltage clamp

and field recordings were registered with a MultiClamp 700B amplifier (Molecular Devices) and signals were filtered at 2 kHz and digitized at 5 kHz. Stimulation and acquisition were controlled with custom software (Igor Pro 6).

Chemicals—NBQX was purchased from Cayman Chemical Company. FSK and DPCPX were ordered from Tocris Bioscience. All chemicals for ACSF, NMDG, internal solutions, and picrotoxin were obtained from MilliporeSigma.

QUANTIFICATION AND STATISTICAL ANALYSIS

Data were analyzed as described in figure legends. Mann-Whitney, Unpaired t test and two-way ANOVA statistical analyses were performed using MATLAB (MathWorks). Tukey's honestly significant difference post hoc test was performed to analyze the statistical significance between groups. For electrophysiology experiments, the Mann-Whitney test was used for $N < 7$ or when data points were not distributed normally as assessed by the Shapiro-Wilk test. For complementary analyses, DiscoRythm R package was used to define the rhythmicity of our dataset as previously done.[122–124] Quantitative data are expressed as mean ± standard error of the mean (SEM) from at least three independent experiments. The individual points displayed in graphs for all western blot and qPCR analyses are replicates for at least 3 animals. Statistically significant differences were established with $*p < 0.05$, $**p < 0.01$ and $***p < 0.001$. See Table S3 for complete statistical information.

Supplementary Material

Refer to Web version on PubMed Central for supplementary material.

ACKNOWLEDGMENTS

We thank the Weill Cornell Medicine Genomics Core facility for providing experimental consultation and results, especially Dr. Paul Zumbo. We thank Aiman Lodhi for her technical help. This work was supported by NIH-R01MH114888.

REFERENCES

1. Farshadi E, van der Horst GTJ, and Chaves I (2020). Molecular links between the circadian clock and the cell cycle. J. Mol. Biol. 432, 3515–3524. 10.1016/j.jmb.2020.04.003. [PubMed: 32304699]
2. Eckel-Mahan K, and Sassone-Corsi P (2013). Metabolism and the circadian clock converge. Physiol. Rev. 93, 107–135. 10.1152/physrev.00016.2012. [PubMed: 23303907]
3. Man K, Loudon A, and Chawla A (2016). Immunity around the clock. Science 354, 999–1003. 10.1126/science.aah4966. [PubMed: 27885005]
4. Holtkamp SJ, Ince LM, Barnoud C, Schmitt MT, Sinturel F, Pilorz V, Pick R, Jemelin S, Mühlstädt M, Boehncke W-H, et al. (2021). Circadian clocks guide dendritic cells into skin lymphatics. Nat. Immunol. 22, 1375–1381. 10.1038/s41590-021-01040-x. [PubMed: 34663979]
5. Lananna B.v., and Musiek ES (2020). The wrinkling of time: aging, inflammation, oxidative stress, and the circadian clock in neurodegeneration. Neurobiol. Dis. 139, 104832. 10.1016/j.nbd.2020.104832. [PubMed: 32179175]
6. Snider KH, Sullivan KA, and Obrietan K (2018). Circadian regulation of hippocampal-dependent memory: circuits, synapses, and molecular mechanisms. Neural Plast. 2018, 7292540–7292613. 10.1155/2018/7292540. [PubMed: 29593785]

7. Ashton A, and Jagannath A (2020). Disrupted sleep and circadian rhythms in schizophrenia and their interaction with dopamine signaling. Front. Neurosci. 14, 636. 10.3389/fnins.2020.00636. [PubMed: 32655359]
8. McCauley JP, Petroccione MA, D'Brant LY, Todd GC, Affinnih N, Wisnoski JJ, Zahid S, Shree S, Sousa AA, de Guzman RM, et al. (2020). Circadian modulation of neurons and astrocytes controls synaptic plasticity in hippocampal area CA1. Cell Rep. 33, 108255. 10.1016/j.celrep.2020.108255. [PubMed: 33053337]
9. Nakatsuka H, and Natsume K (2014). Circadian rhythm modulates long-term potentiation induced at CA1 in rat hippocampal slices. Neurosci. Res. 80, 1–9. 10.1016/j.neures.2013.12.007. [PubMed: 24406747]
10. Jilg A, Lesny S, Peruzki N, Schwegler H, Selbach O, Dehghani F, and Stehle JH (2010). Temporal dynamics of mouse hippocampal clock gene expression support memory processing. Hippocampus 20, 377–388. 10.1002/hipo.20637. [PubMed: 19437502]
11. Kwapis JL, Alaghband Y, Kramár EA, López AJ, Vogel Ciernia A, White AO, Shu G, Rhee D, Michael CM, Montellier E, et al. (2018). Epigenetic regulation of the circadian gene Per1 contributes to age-related changes in hippocampal memory. Nat. Commun. 9, 3323. 10.1038/s41467-018-05868-0. [PubMed: 30127461]
12. Hartsock MJ, and Spencer RL (2020). Memory and the circadian system: identifying candidate mechanisms by which local clocks in the brain may regulate synaptic plasticity. Neurosci. Biobehav. Rev. 118, 134–162. 10.1016/j.neubiorev.2020.07.023. [PubMed: 32712278]
13. Noya SB, Colameo D, Brüning F, Spinnler A, Mircsof D, Opitz L, Mann M, Tyagarajan SK, Robles MS, and Brown SA (2019). The forebrain synaptic transcriptome is organized by clocks but its proteome is driven by sleep. Science 366, eaav2642. 10.1126/science.aav2642. [PubMed: 31601739]
14. Brüning F, Noya SB, Bange T, Koutsouli S, Rudolph JD, Tyagarajan SK, Cox J, Mann M, Brown SA, and Robles MS (2019). Sleep-wake cycles drive daily dynamics of synaptic phosphorylation. Science 366, eaav3617. 10.1126/science.aav3617. [PubMed: 31601740]
15. Hasegawa S, Fukushima H, Hosoda H, Serita T, Ishikawa R, Rokukawa T, Kawahara-Miki R, Zhang Y, Ohta M, Okada S, et al. (2019). Hippocampal clock regulates memory retrieval via Dopamine and PKA-induced GluA1 phosphorylation. Nat. Commun. 10, 5766. 10.1038/s41467-019-13554-y. [PubMed: 31852900]
16. Sehgal A, Price JL, Man B, and Young MW (1994). Loss of circadian behavioral rhythms and per RNA oscillations in the Drosophila mutant timeless. Science 263, 1603–1606. 10.1126/science.8128246. [PubMed: 8128246]
17. Gekakis N, Saez L, Delahaye-Brown A-M, Myers MP, Sehgal A, Young MW, and Weitz CJ (1995). Isolation of timeless by PER protein interaction: defective interaction between timeless protein and long-period mutant PERL. Science 270, 811–815. 10.1126/science.270.5237.811. [PubMed: 7481773]
18. Reppert SM, and Weaver DR (2001). Molecular analysis of mammalian circadian rhythms. Annu. Rev. Physiol. 63, 647–676. 10.1146/annurev.physiol.63.1.647. [PubMed: 11181971]
19. Charrier A, Olliac B, Roubertoux P, and Tordjman S (2017). Clock Genes and altered sleep–wake rhythms: their role in the development of psychiatric disorders. Int. J. Mol. Sci. 18, 938. 10.3390/ijms18050938. [PubMed: 28468274]
20. Musiek ES, and Holtzman DM (2016). Mechanisms linking circadian clocks, sleep, and neurodegeneration. Science 354, 1004–1008. 10.1126/science.aah4968. [PubMed: 27885006]
21. Mansour HA, Wood J, Logue T, Chowdari K.v., Dayal M, Kupfer DJ, Monk TH, Devlin B, and Nimgaonkar VL (2006). Association study of eight circadian genes with bipolar I disorder, schizoaffective disorder and schizophrenia. Genes Brain Behav. 5, 150–157. 10.1111/j.1601-183X.2005.00147.x. [PubMed: 16507006]
22. Yan Q, Nho K, Del-Aguila JL, Wang X, Risacher SL, Fan K-H, Snitz BE, Aizenstein HJ, Mathis CA, Lopez OL, et al. (2021). Genome-wide association study of brain amyloid deposition as measured by Pittsburgh Compound-B (PiB)-PET imaging. Mol. Psychiatry 26, 309–321. 10.1038/s41380-018-0246-7. [PubMed: 30361487]

23. Jaladanki SK, Elmas A, Malave GS, and Huang KL (2021). Genetic dependency of Alzheimer's disease-associated genes across cells and tissue types. Sci. Rep. 11, 12107. 10.1038/s41598-021-91713-2. [PubMed: 34103633]
24. Kurien P, Hsu P-K, Leon J, Wu D, McMahon T, Shi G, Xu Y, Lipzen A, Pennacchio LA, Jones CR, et al. (2019). TIMELESS mutation alters phase responsiveness and causes advanced sleep phase. Proc. Natl. Acad. Sci. USA 116, 12045–12053. 10.1073/pnas.1819110116. [PubMed: 31138685]
25. Bianco JN, Bergoglio V, Lin Y-L, Pillaire M-J, Schmitz A-L, Gilhodes J, Lusque A, Mazières J, Lacroix-Triki M, Roumeliotis TI, et al. (2019). Overexpression of Claspin and Timeless protects cancer cells from replication stress in a checkpoint-independent manner. Nat. Commun. 10, 910. 10.1038/s41467-019-08886-8. [PubMed: 30796221]
26. McFarlane RJ, Mian S, and Dalgaard JZ (2010). The many facets of the Tim-Tipin protein families' roles in chromosome biology. Cell Cycle 9, 700–705. 10.4161/cc.9.4.10676. [PubMed: 20139726]
27. Unsal-Kaçmaz K, Mullen TE, Kaufmann WK, and Sancar A (2005). Coupling of human circadian and cell cycles by the timeless protein. Mol. Cell Biol. 25, 3109–3116. 10.1128/MCB.25.8.3109-3116.2005. [PubMed: 15798197]
28. O'Reilly LP, Watkins SC, and Smithgall TE (2011). An unexpected role for the clock protein timeless in developmental apoptosis. PLoS One 6, e17157. 10.1371/journal.pone.0017157. [PubMed: 21359199]
29. Gotter AL, Manganaro T, Weaver DR, Kolakowski LF, Possidente B, Sriram S, MacLaughlin DT, and Reppert SM (2000). A time-less function for mouse Timeless. Nat. Neurosci. 3, 755–756. 10.1038/77653. [PubMed: 10903565]
30. Kume K, Zylka MJ, Sriram S, Shearman LP, Weaver DR, Jin X, Maywood ES, Hastings MH, and Reppert SM (1999). mCRY1 and mCRY2 are essential components of the negative limb of the circadian clock feedback loop. Cell 98, 193–205. 10.1016/S0092-8674(00)81014-4. [PubMed: 10428031]
31. Mazzoccoli G, Laukkanen MO, Vinciguerra M, Colangelo T, and Colantuoni V (2016). A timeless link between circadian patterns and disease. Trends Mol. Med. 22, 68–81. 10.1016/j.molmed.2015.11.007. [PubMed: 26691298]
32. Sangoram AM, Saez L, Antoch MP, Gekakis N, Staknis D, Whiteley A, Fruechte EM, Vitaterna MH, Shimomura K, King DP, et al. (1998). Mammalian circadian autoregulatory loop. Neuron 21, 1101–1113. 10.1016/S0896-6273(00)80627-3. [PubMed: 9856465]
33. Tischkau SA, Barnes JA, Lin F-J, Myers EM, Barnes JW, Meyer-Bernstein EL, Hurst WJ, Burgoon PW, Chen D, Sehgal A, and Gillette MU (1999). Oscillation and light induction of timeless mRNA in the mammalian circadian clock. J. Neurosci. 19, RC15. 10.1523/JNEUROSCI.19-12-j0005. [PubMed: 10366653]
34. Barnes JW, Tischkau SA, Barnes JA, Mitchell JW, Burgoon PW, Hickok JR, and Gillette MU (2003). Requirement of mammalian Timeless for circadian rhythmicity. Science 302, 439–442. 10.1126/science.1086593. [PubMed: 14564007]
35. Honma S, Ikeda M, Abe H, Tanahashi Y, Namihira M, Honma K, and Nomura M (1998). Circadian oscillation of BMAL1, a partner of a mammalian clock gene Clock,in rat suprachiasmatic nucleus. Biochem. Biophys. Res. Commun. 250, 83–87. 10.1006/bbrc.1998.9275. [PubMed: 9735336]
36. Brancaccio M, Edwards MD, Patton AP, Smyllie NJ, Chesham JE, Maywood ES, and Hastings MH (2019). Cell-autonomous clock of astrocytes drives circadian behavior in mammals. Science 363, 187–192. 10.1126/science.aat4104. [PubMed: 30630934]
37. Besing RC, Rogers CO, Paul JR, Hablitz LM, Johnson RL, McMahon LL, and Gamble KL (2017). GSK3 activity regulates rhythms in hippocampal clock gene expression and synaptic plasticity. Hippocampus 27, 890–898. 10.1002/HIPO.22739. [PubMed: 28556462]
38. Zhang R, Lahens NF, Ballance HI, Hughes ME, and Hogenesch JB (2014). A circadian gene expression atlas in mammals: implications for biology and medicine. Proc. Natl. Acad. Sci. USA 111, 16219–16224. 10.1073/pnas.1408886111. [PubMed: 25349387]
39. Bunger MK, Wilsbacher LD, Moran SM, Clendenin C, Radcliffe LA, Hogenesch JB, Simon MC, Takahashi JS, and Bradfield CA (2000). Mop3 is an essential component of the master circadian

pacemaker in mammals. Cell 103, 1009–1017. 10.1016/S0092-8674(00)00205-1. [PubMed: 11163178]

40. van der Zee EA, Havekes R, Barf RP, Hut RA, Nijholt IM, Jacobs EH, and Gerkema MP (2008). Circadian time-place learning in mice depends on cry genes. Curr. Biol. 18, 844–848. 10.1016/j.cub.2008.04.077. [PubMed: 18514517]
41. Price KH, Dziema H, Aten S, Loeser J, Norona FE, Hoyt K, and Obrietan K (2016). Modulation of learning and memory by the targeted deletion of the circadian clock gene Bmal1 in forebrain circuits. Behav. Brain Res. 308, 222–235. 10.1016/j.bbr.2016.04.027. [PubMed: 27091299]
42. Notaras M, Allen M, Longo F, Volk N, Toth M, Li Jeon N, Klann E, and Colak D (2020). UPF2 leads to degradation of dendritically targeted mRNAs to regulate synaptic plasticity and cognitive function. Mol. Psychiatry 25, 3360–3379. 10.1038/s41380-019-0547-5. [PubMed: 31636381]
43. Bliss TV, and Collingridge GL (1993). A synaptic model of memory: long-term potentiation in the hippocampus. Nature 361, 31–39. 10.1038/361031a0. [PubMed: 8421494]
44. Malenka RC, and Bear MF (2004). LTP and LTD. Neuron 44, 5–21. 10.1016/j.neuron.2004.09.012. [PubMed: 15450156]
45. Poo MM, Pignatelli M, Ryan TJ, Tonegawa S, Bonhoeffer T, Martin KC, Rudenko A, Tsai L-H, Tsien RW, Fishell G, et al. (2016). What is memory? The present state of the engram. BMC Biol. 14, 40. 10.1186/s12915-016-0261-6. [PubMed: 27197636]
46. Salas IH, Callaerts-Vegh Z, Arranz AM, Guix FX, D'Hooge R, Esteban JA, de Strooper B, and Dotti CG (2017). Tetraspanin 6: a novel regulator of hippocampal synaptic transmission and long term plasticity. PLoS One 12, e0171968. 10.1371/JOURNAL.PONE.0171968. [PubMed: 28207852]
47. Stein V, House DRC, Bredt DS, and Nicoll RA (2003). Postsynaptic density-95 mimics and occludes hippocampal long-term potentiation and enhances long-term depression. J. Neurosci. 23, 5503–5506. 10.1523/JNEUROSCI.23-13-05503. [PubMed: 12843250]
48. Young LM, Marzio A, Perez-Duran P, Reid DA, Meredith DN, Roberti D, Star A, Rothenberg E, Ueberheide B, and Pagano M (2015). TIMELESS forms a complex with PARP1 distinct from its complex with TIPIN and plays a role in the DNA damage response. Cell Rep. 13, 451–459. 10.1016/j.celrep.2015.09.017. [PubMed: 26456830]
49. Lerner LK, Holzer S, Kilkenny ML, Švikovic S, Murat P, Schiavone D, Eldridge CB, Bittleston A, Maman JD, Branzei D, et al. (2020). Timeless couples G-quadruplex detection with processing by DDX 11 helicase during DNA replication. EMBO J. 39, e104185. 10.15252/embj.2019104185. [PubMed: 32705708]
50. Eckel-Mahan KL, Patel VR, Mohney RP, Vignola KS, Baldi P, and Sassone-Corsi P (2012). Coordination of the transcriptome and metabolome by the circadian clock. Proc. Natl. Acad. Sci. USA 109, 5541–5546. 10.1073/pnas.1118726109. [PubMed: 22431615]
51. Gjoneska E, Pfenning AR, Mathys H, Quon G, Kundaje A, Tsai L-H, and Kellis M (2015). Conserved epigenomic signals in mice and humans reveal immune basis of Alzheimer's disease. Nature 518, 365–369. 10.1038/nature14252. [PubMed: 25693568]
52. Delhaye S, and Bardoni B (2021). Role of phosphodiesterases in the pathophysiology of neurodevelopmental disorders. Mol. Psychiatry 26, 4570–4582. 10.1038/s41380-020-00997-9. [PubMed: 33414502]
53. Richter W, Menniti FS, Zhang H-T, and Conti M (2013). PDE4 as a target for cognition enhancement. Expert Opin. Ther. Targets 17, 1011–1027. 10.1517/14728222.2013.818656. [PubMed: 23883342]
54. Eckel-Mahan KL, Phan T, Han S, Wang H, Chan GCK, Scheiner ZS, and Storm DR (2008). Circadian oscillation of hippocampal MAPK activity and cAMP: implications for memory persistence. Nat. Neurosci. 11, 1074–1082. 10.1038/nn.2174. [PubMed: 19160506]
55. Lovatt D, Xu Q, Liu W, Takano T, Smith NA, Schnermann J, Tieu K, and Nedergaard M (2012). Neuronal adenosine release, and not astrocytic ATP release, mediates feedback inhibition of excitatory activity. Proc. Natl. Acad. Sci. USA 109, 6265–6270. 10.1073/pnas.1120997109. [PubMed: 22421436]

56. Latini S, and Pedata F (2001). Adenosine in the central nervous system: release mechanisms and extracellular concentrations. J. Neurochem. 79, 463–484. 10.1046/j.1471-4159.2001.00607.x. [PubMed: 11701750]
57. Frey U, Huang Y-Y, and Kandel ER (1993). Effects of cAMP simulate a late stage of LTP in hippocampal CA1 neurons. Science 260, 1661–1664. 10.1126/science.8389057. [PubMed: 8389057]
58. Pockett S, Slack JR, and Peacock S (1993). Cyclic AMP and long-term potentiation in the CA1 region of rat hippocampus. Neuroscience 52, 229–236. 10.1016/0306-4522(93)90151-5. [PubMed: 8383817]
59. Weisskopf MG, Castillo PE, Zalutsky RA, and Nicoll RA (1994). Mediation of hippocampal mossy fiber long-term potentiation by cyclic AMP. Science 265, 1878–1882. 10.1126/science.7916482. [PubMed: 7916482]
60. Diering GH, and Huganir RL (2018). The AMPA receptor code of synaptic plasticity. Neuron 100, 314–329. 10.1016/J.NEURON.2018.10.018. [PubMed: 30359599]
61. Kopec CD, Real E, Kessels HW, and Malinow R (2007). GluR1 links structural and functional plasticity at excitatory synapses. J. Neurosci. 27, 13706–13718. 10.1523/JNEUROSCI.3503-07.2007. [PubMed: 18077682]
62. Zhu JJ, Qin Y, Zhao M, van Aelst L, and Malinow R (2002). Ras and rap control AMPA receptor trafficking during synaptic plasticity. Cell 110, 443–455. 10.1016/S0092-8674(02)00897-8. [PubMed: 12202034]
63. Thiagarajan TC, Lindskog M, and Tsien RW (2005). Adaptation to synaptic inactivity in hippocampal neurons. Neuron 47, 725–737. 10.1016/j.neuron.2005.06.037. [PubMed: 16129401]
64. Malinow R, and Malenka RC (2002). AMPA receptor trafficking and synaptic plasticity. Annu. Rev. Neurosci. 25, 103–126. 10.1146/annurev.neuro.25.112701.142758. [PubMed: 12052905]
65. Lee H-K, Barbarosie M, Kameyama K, Bear MF, and Huganir RL (2000). Regulation of distinct AMPA receptor phosphorylation sites during bidirectional synaptic plasticity. Nature 405, 955–959. 10.1038/35016089. [PubMed: 10879537]
66. Banke TG, Bowie D, Lee H, Huganir RL, Schousboe A, and Traynelis SF (2000). Control of GluR1 AMPA receptor function by cAMP-dependent protein kinase. J. Neurosci. 20, 89–102. 10.1523/JNEUROSCI.20-01-00089. [PubMed: 10627585]
67. Song RS, Massenburg B, Wenderski W, Jayaraman V, Thompson L, and Neves SR (2013). ERK regulation of phosphodiesterase 4 enhances dopamine-stimulated AMPA receptor membrane insertion. Proc. Natl. Acad. Sci. USA 110, 15437–15442. 10.1073/pnas.1311783110. [PubMed: 23986500]
68. Purkey AM, and Dell'Acqua ML (2020). Phosphorylation-dependent regulation of Ca2+-permeable AMPA receptors during hippocampal synaptic plasticity. Front. Synaptic Neurosci. 12, 8. 10.3389/fnsyn.2020.00008. [PubMed: 32292336]
69. Esteban JA, Shi S-H, Wilson C, Nuriya M, Huganir RL, and Malinow R (2003). PKA phosphorylation of AMPA receptor subunits controls synaptic trafficking underlying plasticity. Nat. Neurosci. 6, 136–143. 10.1038/nn997. [PubMed: 12536214]
70. Diering GH, Heo S, Hussain NK, Liu B, and Huganir RL (2016). Extensive phosphorylation of AMPA receptors in neurons. Proc. Natl. Acad. Sci. USA 113, E4920–E4927. 10.1073/pnas.1610631113. [PubMed: 27482106]
71. Havekes R, Park AJ, Tolentino RE, Bruinenberg VM, Tudor JC, Lee Y, Hansen RT, Guercio LA, Linton E, Neves-Zaph SR, et al. (2016). Compartmentalized PDE4A5 signaling impairs hippocampal synaptic plasticity and long-term memory. J. Neurosci. 36, 8936–8946. 10.1523/JNEUROSCI.0248-16.2016. [PubMed: 27559174]
72. Oe Y, Tominaga-Yoshino K, Hasegawa S, and Ogura A (2013). Dendritic spine dynamics in synaptogenesis after repeated LTP inductions: dependence on pre-existing spine density. Sci. Rep. 3, 1957. 10.1038/srep01957. [PubMed: 23739837]
73. Li J, Wilkinson B, Clementel VA, Hou J, O'Dell TJ, and Coba MP (2016). Long-term potentiation modulates synaptic phosphorylation networks and reshapes the structure of the postsynaptic interactome. Sci. Signal. 9, rs8. 10.1126/scisignal.aaf6716. [PubMed: 27507650]

74. Bosch M, and Hayashi Y (2012). Structural plasticity of dendritic spines. Curr. Opin. Neurobiol. 22, 383–388. 10.1016/j.conb.2011.09.002. [PubMed: 21963169]

75. Rawashdeh O, Jilg A, Jedlicka P, Slawska J, Thomas L, Saade A, Schwarzacher SW, and Stehle JH (2014). PERIOD1 coordinates hippocampal rhythms and memory processing with daytime. Hippocampus 24, 712–723. 10.1002/hipo.22262. [PubMed: 24550127]

76. Wardlaw SM, Phan TX, Saraf A, Chen X, and Storm DR (2014). Genetic disruption of the core circadian clock impairs hippocampus-dependent memory. Learn. Mem. 21, 417–423. 10.1101/lm.035451.114. [PubMed: 25034823]

77. Chun LE, Woodruff ER, Morton S, Hinds LR, and Spencer RL (2015). Variations in phase and amplitude of rhythmic clock gene expression across prefrontal cortex, hippocampus, amygdala, and hypothalamic paraventricular and suprachiasmatic nuclei of male and female rats. J. Biol. Rhythms 30, 417–436. 10.1177/0748730415598608. [PubMed: 26271538]

78. Koike N, Hida A, Numano R, Hirose M, Sakaki Y, and Tei H (1998). Identification of the mammalian homologues of the Drosophila timeless gene, Timeless1. FEBS Lett. 441, 427–431. 10.1016/S0014-5793(98)01597-X. [PubMed: 9891984]

79. Takumi T, Nagamine Y, Miyake S, Matsubara C, Taguchi K, Takekida S, Sakakida Y, Nishikawa K, Kishimoto T, Niwa S, et al. (1999). A mammalian ortholog of Drosophila timeless, highly expressed in SCN and retina, forms a complex with mPER1. Gene Cell. 4, 67–75. 10.1046/j.1365-2443.1999.00238.x.

80. Zylka MJ, Shearman LP, Levine JD, Jin X, Weaver DR, and Reppert SM (1998). Molecular analysis of mammalian timeless. Neuron 21, 1115–1122. 10.1016/S0896-6273(00)80628-5. [PubMed: 9856466]

81. Engelen E, Janssens RC, Yagita K, Smits VAJ, van der Horst GTJ, and Tamanini F (2013). Mammalian TIMELESS is involved in period determination and DNA damage-dependent phase advancing of the circadian clock. PLoS One 8, e56623. 10.1371/journal.pone.0056623. [PubMed: 23418588]

82. Stephan FK, and Kovacevic NS (1978). Multiple retention deficit in passive avoidance in rats is eliminated by suprachiasmatic lesions. Behav. Biol. 22, 456–462. 10.1016/S0091-6773(78)92565-8. [PubMed: 567972]

83. Phan TX, Chan GC-K, Sindreu CB, Eckel-Mahan KL, and Storm DR (2011). The diurnal oscillation of MAP (Mitogen-Activated protein) kinase and adenylyl cyclase activities in the Hippocampus depends on the suprachiasmatic nucleus. J. Neurosci. 31, 10640–10647. 10.1523/JNEUROSCI.6535-10.2011. [PubMed: 21775607]

84. Eckel-Mahan KL, and Storm DR (2009). Circadian rhythms and memory: not so simple as cogs and gears. EMBO Rep. 10, 584–591. 10.1038/embor.2009.123. [PubMed: 19465890]

85. Benna C, Bonaccorsi S, Wülbeck C, Helfrich-Förster C, Gatti M, Kyriacou CP, Costa R, and Sandrelli F (2010). Drosophila timeless2 is required for chromosome stability and circadian photoreception. Curr. Biol. 20, 346–352. 10.1016/j.cub.2009.12.048. [PubMed: 20153199]

86. Sun X, Zhao Y, and Wolf ME (2005). Dopamine receptor stimulation modulates AMPA receptor synaptic insertion in prefrontal cortex neurons. J. Neurosci. 25, 7342–7351. 10.1523/JNEUROSCI.4603-04.2005. [PubMed: 16093384]

87. Oh MC, Derkach VA, Guire ES, and Soderling TR (2006). Extrasynaptic membrane trafficking regulated by GluR1 serine 845 phosphorylation primes AMPA receptors for long-term potentiation. J. Biol. Chem. 281, 752–758. 10.1074/jbc.M509677200. [PubMed: 16272153]

88. Man H-Y, Sekine-Aizawa Y, and Huganir RL (2007). Regulation of α-amino-3-hydroxy-5-methyl-4-isoxazolepropionic acid receptor trafficking through PKA phosphorylation of the Glu receptor 1 subunit. Proc. Natl. Acad. Sci. USA 104, 3579–3584. 10.1073/pnas.0611698104. [PubMed: 17360685]

89. Yang Y, Wang XB, Frerking M, and Zhou Q (2008). Delivery of AMPA receptors to perisynaptic sites precedes the full expression of long-term potentiation. Proc. Natl. Acad. Sci. USA 105, 11388–11393. 10.1073/pnas.0802978105. [PubMed: 18682558]

90. He K, Song L, Cummings LW, Goldman J, Huganir RL, and Lee H-K (2009). Stabilization of Ca 2+ -permeable AMPA receptors at perisynaptic sites by GluR1-S845 phosphorylation. Proc. Natl. Acad. Sci. USA 106, 20033–20038. 10.1073/pnas.0910338106. [PubMed: 19892736]

91. Diering GH, Gustina AS, and Huganir RL (2014). PKA-GluA1 coupling via AKAP5 controls AMPA receptor phosphorylation and cell-surface targeting during bidirectional homeostatic plasticity. Neuron 84, 790–805. 10.1016/j.neuron.2014.09.024. [PubMed: 25451194]
92. Park P, Georgiou J, Sanderson TM, Ko K-H, Kang H, Kim JI, Bradley CA, Bortolotto ZA, Zhuo M, Kaang B-K, and Collingridge GL (2021). PKA drives an increase in AMPA receptor unitary conductance during LTP in the hippocampus. Nat. Commun. 12, 413. 10.1038/s41467-020-20523-3. [PubMed: 33462202]
93. Silva AJ, Kogan JH, Frankland PW, and Kida S (1998). Creb and memory. Annu. Rev. Neurosci. 21, 127–148. 10.1146/annurev.neuro.21.1.127. [PubMed: 9530494]
94. Carlezon WA Jr., Duman RS, and Nestler EJ (2005). The many faces of CREB. Trends Neurosci. 28, 436–445. 10.1016/j.tins.2005.06.005. [PubMed: 15982754]
95. Li Y-F, Cheng Y-F, Huang Y, Conti M, Wilson SP, O'Donnell JM, and Zhang H-T (2011). Phosphodiesterase-4D knock-out and RNA interference-mediated knock-down enhance memory and increase hippocampal neurogenesis via increased cAMP signaling. J. Neurosci. 31, 172–183. 10.1523/JNEUROSCI.5236-10.2011. [PubMed: 21209202]
96. Tropea D, Hardingham N, Millar K, and Fox K (2018). Mechanisms underlying the role of DISC1 in synaptic plasticity. J. Physiol. 596, 2747–2771. 10.1113/JP274330. [PubMed: 30008190]
97. Barco A, Alarcon JM, and Kandel ER (2002). Expression of constitutively active CREB protein facilitates the late phase of long-term potentiation by enhancing synaptic capture. Cell 108, 689–703. 10.1016/S0092-8674(02)00657-8. [PubMed: 11893339]
98. Tibbo AJ, and Baillie GS (2020). Phosphodiesterase 4B: master regulator of brain signaling. Cells 9, 1254. 10.3390/cells9051254. [PubMed: 32438615]
99. McGirr A, Lipina T.v., Mun H-S, Georgiou J, Al-Amri AH, Ng E, Zhai D, Elliott C, Cameron RT, Mullins JGL, et al. (2016). Specific inhibition of phosphodiesterase-4B results in anxiolysis and facilitates memory acquisition. Neuropsychopharmacology 41, 1080–1092. 10.1038/npp.2015.240. [PubMed: 26272049]
100. Campbell SL, van Groen T, Kadish I, Smoot LHM, and Bolger GB (2017). Altered phosphorylation, electrophysiology, and behavior on attenuation of PDE4B action in hippocampus. BMC Neurosci. 18, 77. 10.1186/s12868-017-0396-6. [PubMed: 29197324]
101. Rutten K, Wallace TL, Works M, Prickaerts J, Blokland A, Novak TJ, Santarelli L, and Misner DL (2011). Enhanced long-term depression and impaired reversal learning in phosphodiesterase 4B-knockout (PDE4B−/−) mice. Neuropharmacology 61, 138–147. 10.1016/j.neuropharm.2011.03.020. [PubMed: 21458469]
102. Cermakian N, and Sassone-Corsi P (2000). Multilevel regulation of the circadian clock. Nat. Rev. Mol. Cell Biol. 1, 59–67. 10.1038/35036078. [PubMed: 11413490]
103. Kim SH, Lee KH, Kim DY, Kwak E, Kim S, and Kim KT (2015). Rhythmic control of mRNA stability modulates circadian amplitude of mouse Period3 mRNA. J. Neurochem. 132, 642–656. 10.1111/JNC.13027. [PubMed: 25581122]
104. Penzes P, Cahill ME, Jones KA, VanLeeuwen J-E, and Woolfrey KM (2011). Dendritic spine pathology in neuropsychiatric disorders. Nat. Neurosci. 14, 285–293. 10.1038/nn.2741. [PubMed: 21346746]
105. Segal M (2005). Dendritic spines and long-term plasticity. Nat. Rev. Neurosci. 6, 277–284. 10.1038/nrn1649. [PubMed: 15803159]
106. Liston C, Cichon JM, Jeanneteau F, Jia Z, Chao MV, and Gan W-B (2013). Circadian glucocorticoid oscillations promote learning-dependent synapse formation and maintenance. Nat. Neurosci. 16, 698–705. 10.1038/nn.3387. [PubMed: 23624512]
107. Ikeda M, Hojo Y, Komatsuzaki Y, Okamoto M, Kato A, Takeda T, and Kawato S (2015). Hippocampal spine changes across the sleep–wake cycle: corticosterone and kinases. J. Endocrinol. 226, M13–M27. 10.1530/JOE-15-0078. [PubMed: 26034071]
108. Wei H, and Stengl M (2011). Light affects the branching pattern of peptidergic circadian pacemaker neurons in the brain of the cockroach *Leucophaea maderae*. J. Biol. Rhythms 26, 507–517. 10.1177/0748730411419968. [PubMed: 22215609]
109. Fernández MP, Berni J, and Ceriani MF (2008). Circadian remodeling of neuronal circuits involved in rhythmic behavior. PLoS Biol. 6, 69. 10.1371/journal.pbio.

110. Krzeptowski W, Hess G, and Pyza E (2018). Circadian plasticity in the brain of insects and rodents. Front. Neural Circuits 12, 32. 10.3389/fncir.2018.00032. [PubMed: 29770112]
111. Gerstner JR, and Yin JCP (2010). Circadian rhythms and memory formation. Nat. Rev. Neurosci. 11, 577–588. 10.1038/nrn2881. [PubMed: 20648063]
112. Yang Z, Matsumoto A, Nakayama K, Jimbo EF, Kojima K, Nagata K.i., Iwamoto S, and Yamagata T (2016). Circadian-relevant genes are highly polymorphic in autism spectrum disorder patients. Brain Dev. 38, 91–99. 10.1016/j.braindev.2015.04.006. [PubMed: 25957987]
113. Chauhan R, Chen K-F, Kent BA, and Crowther DC (2017). Central and peripheral circadian clocks and their role in Alzheimer's disease. Dis. Model. Mech. 10, 1187–1199. 10.1242/dmm.030627. [PubMed: 28993311]
114. Parekh PK, Becker-Krail D, Sundaravelu P, Ishigaki S, Okado H, Sobue G, Huang Y, and McClung CA (2018). Altered GluA1 (Gria1) function and accumbal synaptic plasticity in the ClockD19 model of bipolar mania. Biol. Psychiatry 84, 817–826. 10.1016/j.biopsych.2017.06.022. [PubMed: 28780133]
115. Gurney ME (2019). Genetic association of phosphodiesterases with human cognitive performance. Front. Mol. Neurosci. 12, 22. 10.3389/fnmol.2019.00022. [PubMed: 30800055]
116. Braun NN, Reutiman TJ, Lee S, Folsom TD, and Fatemi SH (2007). Expression of phosphodiesterase 4 is altered in the brains of subjects with autism. Neuroreport 18, 1841–1844. 10.1097/WNR.0b013e3282f16dca. [PubMed: 18090323]
117. Inaguma Y, Ito H, Hara A, Iwamoto I, Matsumoto A, Yamagata T, Tabata H, and Nagata KI (2015). Morphological characterization of mammalian Timeless in the mouse brain development. Neurosci. Res. 92, 21–28. 10.1016/j.neures.2014.10.017. [PubMed: 25448545]
118. Madisen L, Zwingman TA, Sunkin SM, Oh SW, Zariwala HA, Gu H, Ng LL, Palmiter RD, Hawrylycz MJ, Jones AR, et al. (2010). A robust and high-throughput Cre reporting and characterization system for the whole mouse brain. Nat. Neurosci. 13, 133–140. 10.1038/nn.2467. [PubMed: 20023653]
119. Schmittgen TD, and Livak KJ (2008). Analyzing real-time PCR data by the comparative CT method. Nat. Protoc. 3, 1101–1108. 10.1038/nprot.2008.73. [PubMed: 18546601]
120. Notaras M, Hill R, Gogos JA, and van den Buuse M (2016). BDNF Val66Met genotype determines hippocampus-dependent behavior via sensitivity to glucocorticoid signaling. Mol. Psychiatry 21, 730–732. 10.1038/mp.2015.152. [PubMed: 26821977]
121. Park KA, Ribic A, Laage Gaupp FM, Coman D, Huang Y, Dulla CG, Hyder F, and Biederer T (2016). Excitatory synaptic drive and feedforward inhibition in the hippocampal CA3 circuit are regulated by SynCAM 1. J. Neurosci. 36, 7464–7475. 10.1523/JNEUROSCI.0189-16.2016. [PubMed: 27413156]
122. Carlucci M, Kri S Ci Unas A, Li H, Gibas P, Koncevi Cius K, Petronis A, Oh G, and Kelso J (2019). DiscoRhythm: an easy-to-use web application and R package for discovering rhythmicity. Bioinformatics 36, 1952–1954. 10.1093/bioinformatics/btz834. [PubMed: 31702788]
123. Cornelissen G (2014). Cosinor-based rhythmometry. Theor. Biol. Med. Model. 11, 16. 10.1186/1742-4682-11-16. [PubMed: 24725531]
124. Hughes ME, Hogenesch JB, and Kornacker K (2010). JTK_CYCLE: an efficient non-parametric algorithm for detecting rhythmic components in genome-scale datasets. J. Biol. Rhythms 25, 372–380. 10.1177/0748730410379711. [PubMed: 20876817]

Highlights

- TIMELESS displays region-specific circadian patterns of expression in the adult mouse brain
- TIMELESS is a transcriptional regulator that modulates PDE4B/cAMP levels in hippocampus
- Disrupted *Timeless* enhances GluA1 phosphorylation, spine density, and basal neurotransmission
- *Timeless* deletion attenuates long-term potentiation and contextual fear memory

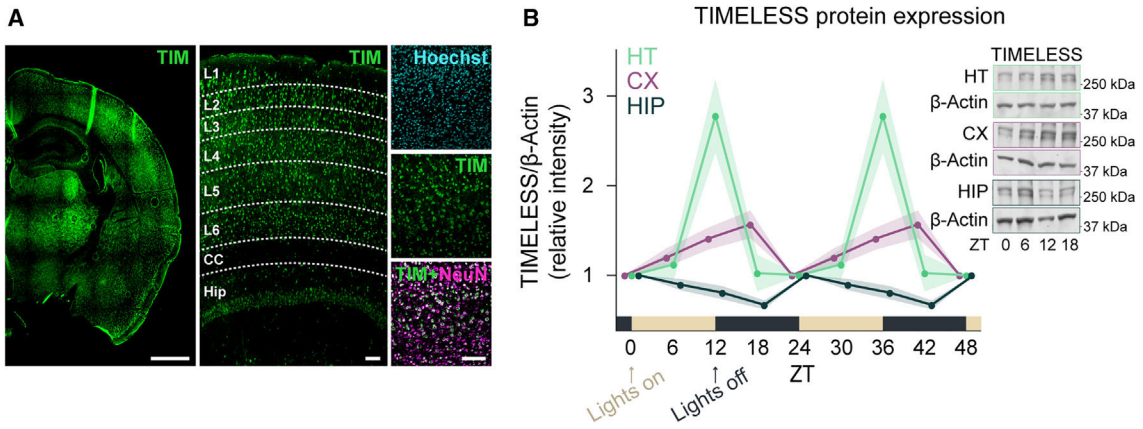

Figure 1. TIMELESS expression displays circadian oscillation in different areas of the adult mouse brain

(A) TIMELESS is expressed in all cortical layers and the hippocampus in the adult mouse brain. TIMELESS co-localizes with the neuronal marker NeuN (magenta).

(B) Quantification of TIMELESS protein at different time points in different brain areas; all values were normalized to β-actin first and then normalized to each brain area at time ZT0. Hypothalamus (green) shows a peak of TIMELESS expression at ZT12 (ZT0 vs. ZT12, **p = 0.001; ZT6 vs. ZT12, **p = 0.009; ZT12 vs. ZT18, **p = 0.004; two-way ANOVA). In the cortex (magenta), TIMELESS expression enhances as the dark phase approaches (ZT0 vs. ZT12, *p = 0.035; two-way ANOVA). In the dark phase, the hippocampus (blue) shows a decrease in TIMELESS expression, in contrast to the other two brain regions, which show positive oscillations (ZT0 vs. ZT18, ***p < 0.001; ZT0 vs. ZT12, *p = 0.012; ZT6 vs. ZT18, *p = 0.019; two-way ANOVA). ZT is for zeitgeber time and is determined by the light and dark cycle (ZT0 denotes time of lights on and ZT12 denotes lights off). Scale bars, 1 mm (whole brain section) and 100 μm (cortex and hippocampus). Data are represented as the mean ± SEM; SEM is depicted as shadings; n = 5–6 WT animals in each time point. Blots shown are representative of 10 independent experiments; *p < 0.05, **p < 0.01, and ***p < 0.001.

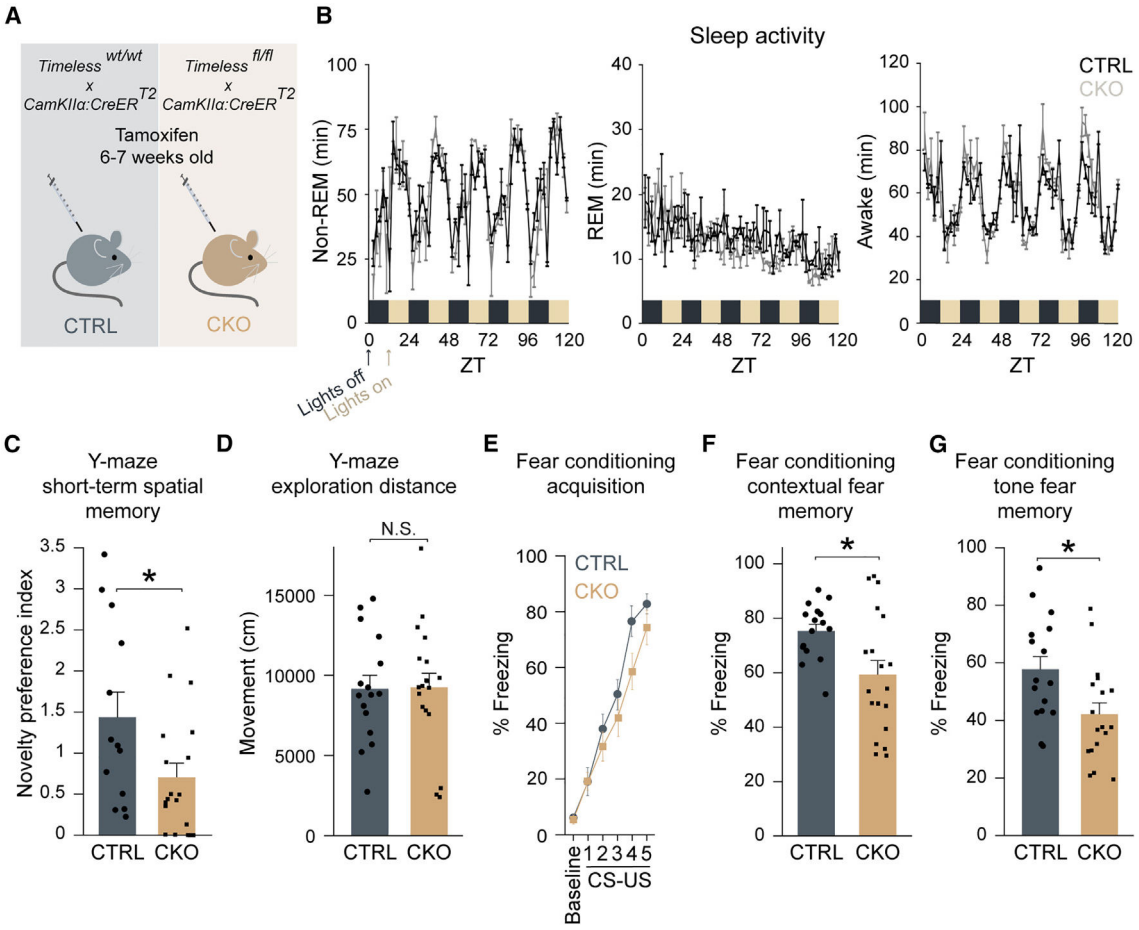

Figure 2. *Timeless* deletion impairs hippocampal-dependent memory in adult mice at ZT12

(A) Schematic of experimental design. *Timeless*$^{fl/fl}$ mice were crossed with *CaMKIIα*:*CreER*^{T2} mice and at 6–7 weeks were treated with tamoxifen (5 days, 200 kg/mg) to induce *Timeless* deletion (CKO). *Timeless*$^{wt/wt}$ crossed with *CaMKIIα*:*CreER*^{T2} and dosed with tamoxifen served as control (CTRL).

(B) Quantification of sleep-wake states in CTRL (n = 2 animals) and CKO (n = 3 animals) revealed no significant differences in non-REM, REM, and awake states over a 5-day period displayed in 24-h bins. On the x axis, yellow bars indicate animal quiescent states during lights on and black bars denote wakeful states during lights off. Cross-correlation analysis showed no phase shift in CKO mice, suggesting that sleep-wake activity is not altered in *Timeless* CKO mice. Data are shown as the mean ± SEM of the time spent in specific sleep-wake states in minutes.

(C–G) *Timeless* CKO mice exhibited impaired short-term and fear memory at ZT12. (C) Compared with CTRL mice, *Timeless* CKO exhibited a substantial decrease in preference for the “novel” arm vs. the “familiar” arm (CTRL n = 14 and CKO n = 19; *p = 0.025, Mann-Whitney test). (D) Exploration distances in the Y maze were not significantly different between the groups (CTRL n = 14 and CKO n = 19; p = 0.706, Mann-Whitney test), indicating that this phenotype is not an effect of different exploration distances between CTRL and CKO. (E) CKO mice were able to learn tone-shock association to a similar degree compared with CTRL, indicating that learning acquisition is intact (CTRL n

= 16 and CKO n = 18; N.S., two-way ANOVA). (F and G) At ZT12, *Timeless* CKO mice exhibited reduced freezing behavior when exposed to the fear context (CTRL n = 16 and CKO n = 19; *p = 0.021, Mann-Whitney test) and in the tone test phase (CTRL n = 16 and CKO n = 18; *p = 0.022, Mann-Whitney test), suggesting that *Timeless* CKO mice display impaired memory. Individual data points representing the number of animals are shown for all experiments. Experiments were performed at ZT12. Data are represented as the mean ± SEM; N.S. denotes non-significant, *p < 0.05.

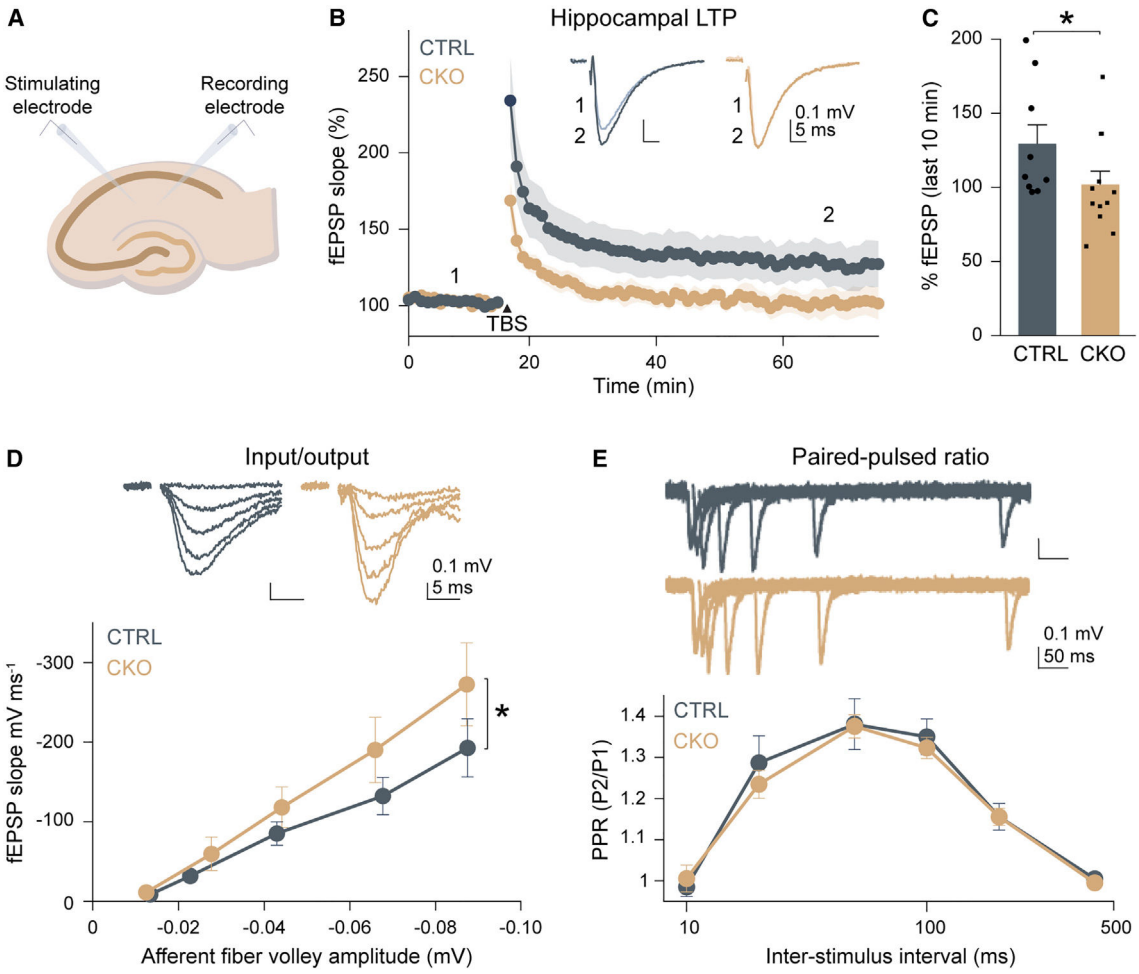

Figure 3. *Timeless* ablation compromises hippocampal synaptic plasticity

(A) Schematic of electrophysiological field recordings of Schaffer-collateral synapses in acute hippocampal slices.

(B) Time course of LTP induced by theta-burst stimulation; representative traces (top). The number 1 denotes baseline (light color) and 2 denotes last 10 min (dark color).

(C) Quantification of the last 10 min of field excitatory post-synaptic potentials (fEPSPs) revealed a significant reduction in LTP magnitude in CKO animals compared with CTRL (CTRL n = 9 slices/4 animals; CKO n = 12 slices/5 animals; *p = 0.033, Mann-Whitney test).

(D) Input-output analysis of Schaffer-collateral fEPSPs revealed enhanced synaptic strength in the CKO condition compared with the CTRL group (CTRL n = 11 slices/4 animals; CKO n = 11 slices/5 animals; *p = 0.027, Mann-Whitney test).

(E) Paired-pulse ratio analysis across varying interstimulus intervals showed no differences in presynaptic release (CTRL n = 9 slices/4 animals; CKO n = 10 slices/5 animals; N.S., unpaired t test). Individual data points represent the number of slices from the number of animals indicated (n). Experiments were performed at ZT12. Data are represented as the mean ± SEM. N.S. denotes non-significant, *p < 0.05.

A

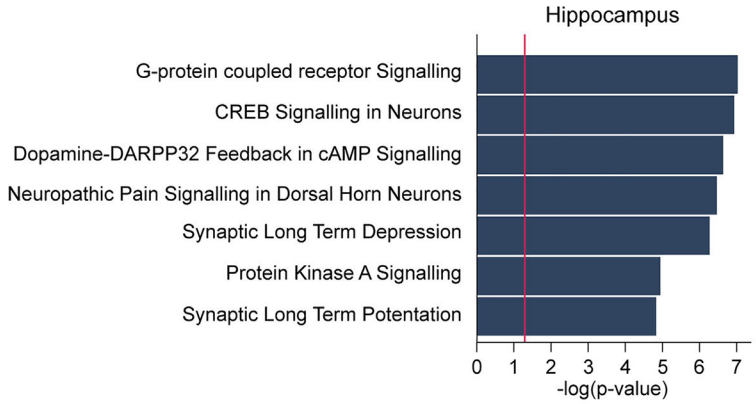

B

Chromosome	Start	End	Gene name	Gene description	Genomic location
chr4	102494013	102494407	*Pde4b*	phosphodiesterase 4B, cAMP specific	Intron
chr3	35224914	35225302	*Mir6378*	microRNA 6378	Intergenic
chr4	43046370	43046712	*Fam214b*	family with sequence similarity 214	Promoter-TSS
chr3	153524429	153525098	*St6galnac3*	ST6	Intron
chr4	151738096	151738361	*Camta1*	calmodulin binding transcription activator 1	Intron
chr4	32356629	32357069	*Bach2*	basic leucine zipper transcription factor 2	Intergenic
chr18	37813535	37813671	*Pcdhgc4*	protocadherin gamma subfamily C, 4	Intron

C

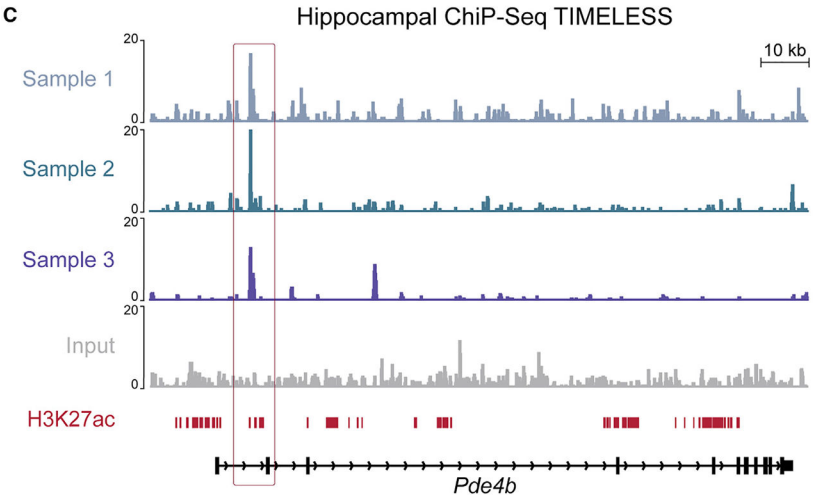

Figure 4. TIMELESS is a chromatin-bound protein that is enriched in enhancer regions of synaptic plasticity genes and pathways in the hippocampus

(A and B) GREAT (Genomic Regions Enrichment of Annotations Tool) analysis of TIMELESS ChIP-seq peaks in WT mouse hippocampal tissue. (A) Top seven pathways enriched for TIMELESS bound genes in the hippocampal region of WT mice using ingenuity pathway analysis (IPA). The significance threshold for pathway enrichment is $p < 0.05$ −log10(p value), corresponding to >1.3 on the x axis of the plot, marked by a red line. (B) Principal candidate peak genes overlapping with active enhancers in adult mouse hippocampus.[51]

(C) Bigwig intensities of TIMELESS ChIP-seq assays adjacent to the *Pde4b* gene performed in hippocampal tissues from n = 3 independent samples (different shades of blue) and non-immunoprecipitated fractions (input, in gray). H3K27ac-bound regions are active sites of transcription, shown in red.[51]

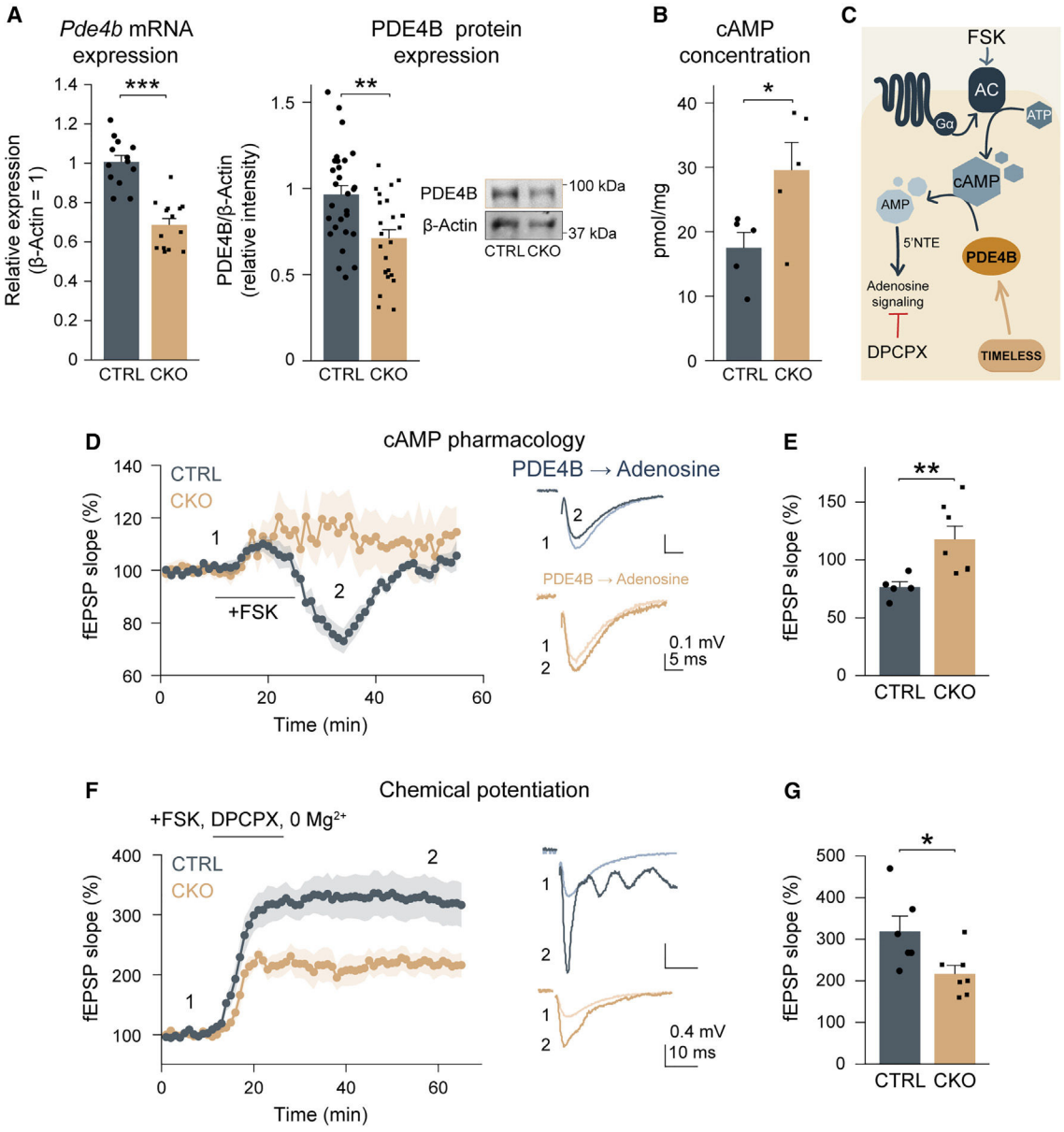

Figure 5. *Timeless* deletion alters PDE4B expression, cAMP levels, and synaptic transmission in hippocampus

(A) TIMELESS upregulates *Pde4b* transcription and thereby PDE4B protein levels in hippocampus. At ZT12, *Pde4b* mRNA levels and PDE4B protein levels are reduced in *Timeless* CKO relative to CTRL (qRT-PCR for mRNA: CTRL n = 9, CKO n = 5; ***p < 0.001, Mann-Whitney test. Western blot for protein: CTRL n = 7, CKO n = 7; **p = 0.014, Mann-Whitney test).

(B) TIMELESS negatively regulates cAMP concentration in hippocampus. ELISA showed that cAMP concentration was elevated in hippocampus of CKO compared with CTRL (CTRL n = 5, CKO n = 6; *p = 0.027, Mann-Whitney test).

(C) Schematic of PDE4B/cAMP signaling cascade in neurons.

(D and E) Pharmacological treatments that target cAMP activation to promote synaptic potentiation demonstrated that TIMELESS can affect synaptic transmission. (D) CKO mice showed a moderate potentiation induced by bath application of 50 μM FSK (an adenylate cyclase activator) compared with the CTRL group, which displayed a dramatic transient decrease in neurotransmission. PDE4B-mediated cAMP degradation to AMP and generation of adenosine via 5′-nucleotidase can lead to suppression of neurotransmitter release,[55,56] as seen in CTRL mice. Reduced PDE4B activity in CKO may explain the absence of transient depression in neurotransmission. (E) Quantification of mean fEPSP slope at 30–35 min of recording (CTRL n = 5 slices/4 animals; CKO n = 7 slices/4 animals; **p = 0.005, Mann-Whitney test).

(F) *Timeless* deletion led to a reduced chemical potentiation induced by co-application of 50 μM FSK and 100 nM DPCPX (an A1 receptor antagonist) in nominal magnesium (FSK, DPCPX, 0 Mg^{2+}) in slices from CKO mice relative to CTRL slices.

(G) Quantification of mean fEPSP slope at 60–65 min of recording (CTRL n = 6 slices/4 animals; CKO n = 7 slices/4 animals; *p = 0.035, Mann-Whitney test). Individual points represent replicates from the number of animals indicated (n). All samples were collected and experiments performed at ZT12. Data are represented as the mean ± SEM. *p < 0.05, **p < 0.01, and ***p < 0.001. In (C), AC denotes adenylate cyclase, ATP denotes adenosine triphosphate, AMP denotes adenosine monophosphate, cAMP denotes cyclic AMP, PDE4B denotes phosphodiesterase 4B, FSK denotes forskolin, 5′NTE denotes 5′-nucleotidase, and DPCPX stands for the selective A1 adenosine receptor antagonist. In (D) and (F), representative traces of baseline fEPSPs are in light color and after treatment in dark color. The number 1 denotes baseline and 2 denotes treatment.

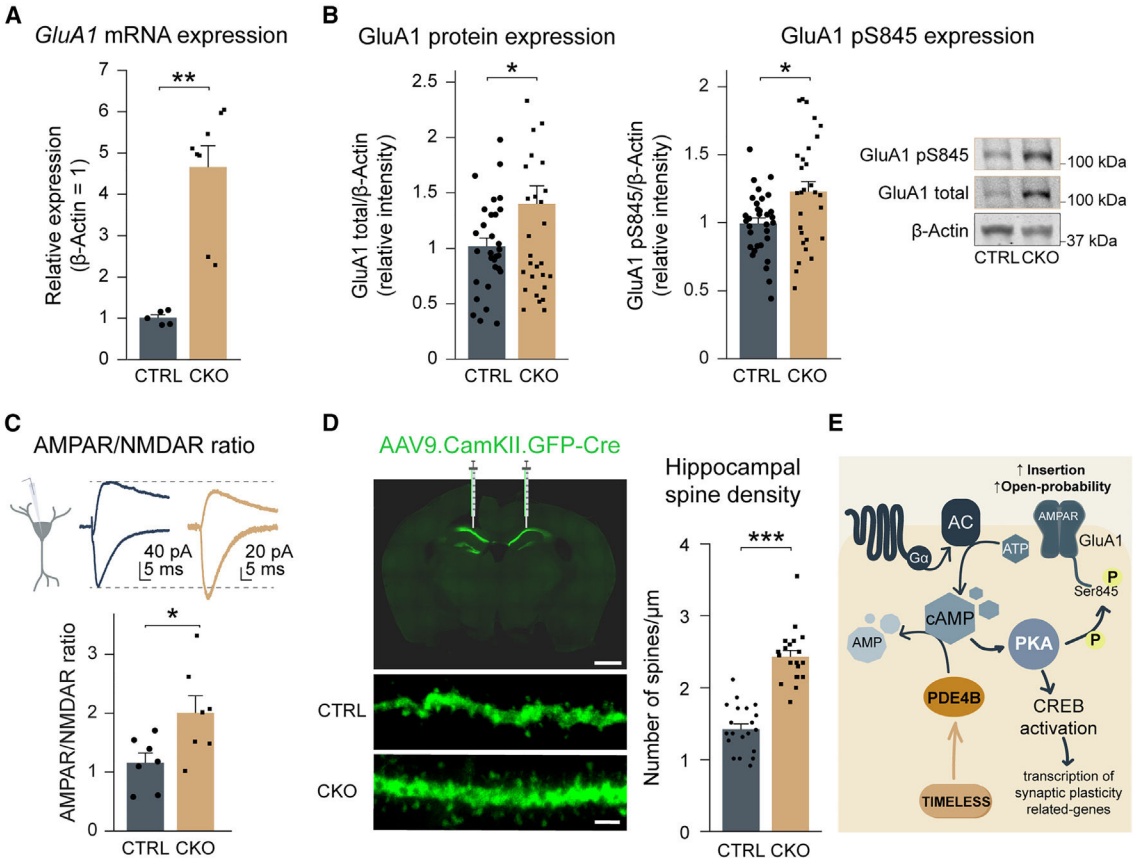

Figure 6. TIMELESS deficiency enhances AMPAR properties and increases spine density in hippocampus

(A) *GluA1* mRNA levels are increased in *Timeless* CKO mice (CTRL n = 3, CKO n = 5; **p = 0.001, Mann-Whitney test).

(B) GluA1 total protein levels and GluA1 phosphorylation of residue S845 are increased in CKO relative to CTRL (CTRL n = 4, CKO n = 4; total GluA1, *p = 0.018, and GluA1 pS845, *p = 0.013, Mann-Whitney test).

(C) *Timeless* CKO mice showed elevated AMPAR/NMDAR ratio relative to CTRL slices (CTRL n = 7 cells/3 animals, CKO n = 7 cells/3 animals; *p = 0.026, Mann-Whitney test).

(D) Spine density is associated with AMPAR density and synaptic plasticity.[71,72,73] CTRL and CKO mice were bilaterally injected with *CaMKIIα*.GFP-CRE virus in CA1 in the hippocampus to label dendritic spines. Representative images of the injections in CA1 neurons labeled with GFP are shown. CKO CA1 dendrites showed a significant increase in the number of spines per 20-µm segment relative to CTRL dendrites (CTRL n = 20 dendrites from 4 mice, CKO n = 33 dendrites from 4 mice; ***p < 0.001, Mann-Whitney test).

(E) Schematic of cAMP/PKA/AMPAR signaling cascade in neurons. Individual points represent replicates from the number of animals indicated (n). All samples were collected, and experiments were performed at ZT12. Data are represented as the mean ± SEM. N.S. denotes non-significant, *p < 0.05, **p < 0.01, and ***p < 0.001. Scale bars, 1 mm, 10× (top in D), and 2 µm, 63×, zoom 4.5 (bottom in D). In (E), AC denotes adenylate cyclase, ATP denotes adenosine triphosphate, AMP stands for adenosine monophosphate, cAMP denotes cyclic AMP, PDE4B denotes phosphodiesterase 4B, PKA stands for protein kinase

A, CREB denotes cAMP response element binding, AMPAR stands for AMPA receptor, P in yellow circle denotes phosphorylation.

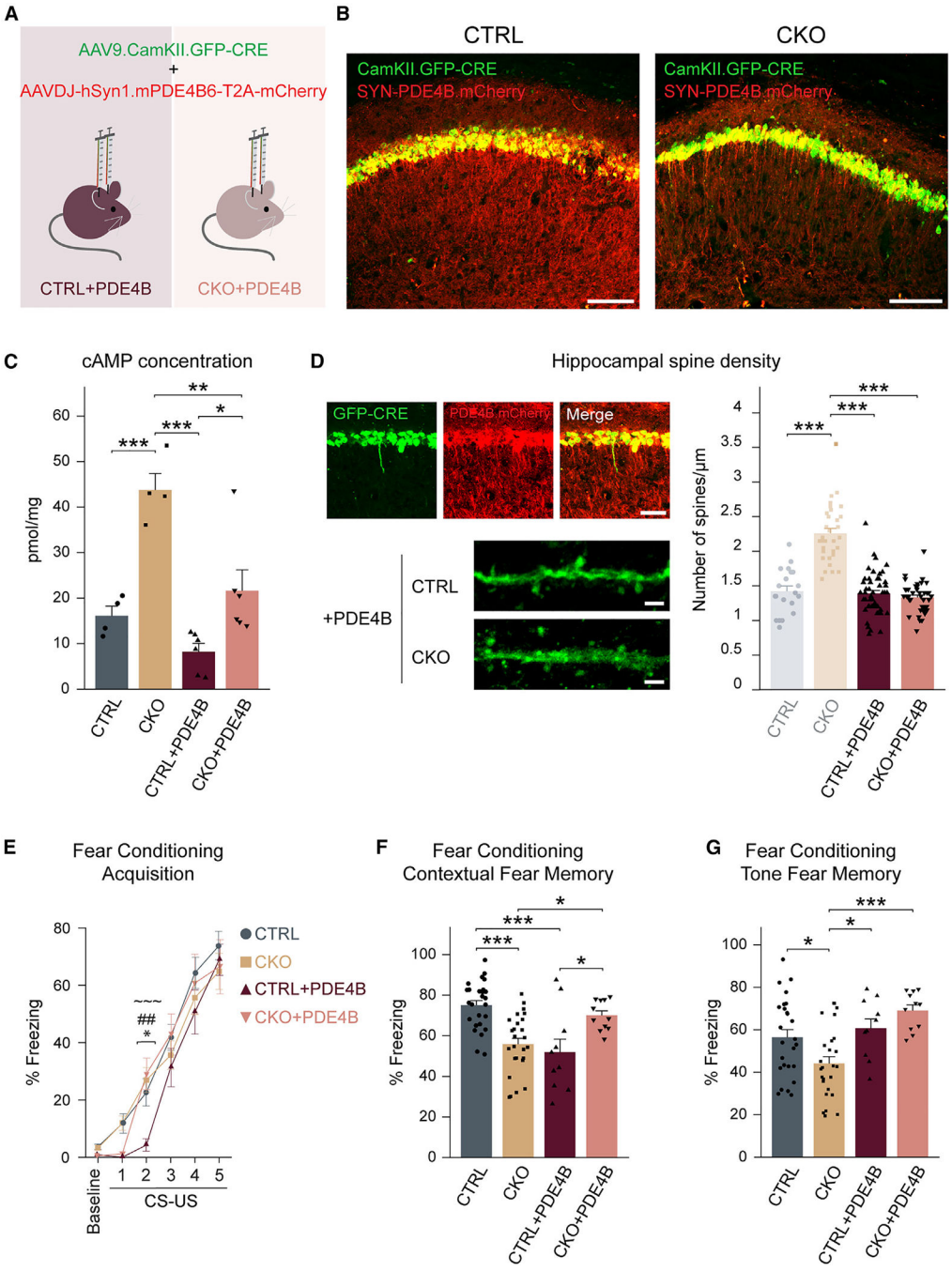

Figure 7. PDE4B supplementation in *Timeless* CKO mice rescues contextual fear memory and spine density phenotypes through normalization of cAMP levels

(A) Schematic of adenovirus-mediated PDE4B delivery to hippocampus in CTRL and CKO mice. To induce *Timeless* deletion and overexpression of PDE4B in excitatory neurons simultaneously, mice were bilaterally injected with a mix of *CaMKIIα*.GFP-CRE and hSyn1.mPDE4B6-T2A-mCherry (ratio 1:3).

(B) Representative images of the CA1 region that validate virus transduction and dendrite labeling. GFP^+ cells expressing CRE and $mCherry^+$ cells expressing isoform 6 of PDE4B are shown.

(C) PDE4B supplementation normalizes cAMP levels in CKO mice. ELISA was performed in hippocampal tissue from all four groups. Hippocampal cAMP levels in CKO + PDE4B mice are comparable to CTRL levels, showing a significant decrease relative to CKO mice (CTRL n = 4, CKO n = 4, CTRL + PDE4B n = 6, CKO + PDE4B n = 6; CTRL vs. CKO, ***p < 0.001; CKO vs. CTRL + PDE4B, ***p < 0.001; CKO vs. CKO + PDE4B, **p = 0.001; CTRL + PDE4B vs. CKO + PDE4B, *p = 0.0357; two-way ANOVA).
(D) No difference in spine densities of hippocampal neurons was found between CTRL mice and CKO supplemented with PDE4B mice. CTRL and CKO data depicted in the graph were previously displayed in Figure 6D and are used here for statistical comparison (CTRL n = 20 dendrites, CKO n = 33 dendrites, CTRL + PDE4B n = 54 dendrites, CKO + PDE4B n = 43 dendrites; CTRL vs. CKO, ***p < 0.001; CKO vs. CTRL + PDE4B, ***p < 0.001; CKO vs. CKO + PDE4B, ***p < 0.001; two-way ANOVA). Representative images of dendritic spines in the CTRL + PDE4B and CKO + PDE4B groups are shown.
(E–G) PDE4B supplementation in *Timeless* CKO hippocampus (CKO + PDE4B) prevented memory deficits. (E) Fear acquisition was not different among the four experimental groups by the last tone-shock pairing (CTRL n = 26, CKO n = 26, CTRL + PDE4B n = 10, CKO + PDE4B n = 12; N.S., two-way ANOVA). The CTRL + PDE4B group showed a learning delay during the second tone-shock association (CTRL + PDE4B vs. CTRL, *p = 0.0308; CTRL + PDE4B vs. CKO, $^{\sim\sim\sim}$p < 0.001; CTRL + PDE4B vs. CKO + PDE4B, $^{\#\#}$p = 0.001; two-way ANOVA). (F and G) In the contextual fear memory test, CKO + PDE4B mice performed similar to CTRL mice and exhibited increased freezing behavior compared with CKO mice (CTRL n = 26, CKO n = 26, CTRL + PDE4B n = 10, CKO + PDE4B n = 11; CTRL vs. CKO, ***p < 0.001; CTRL vs. CTRL + PDE4B, ***p < 0.001; CKO vs. CKO + PDE4B, *p = 0.0332; CTRL + PDE4B vs. CKO + PDE4B, *p = 0.0043; two-way ANOVA). Similarly, in the tone memory test, freezing percentage of CKO + PDE4B mice was comparable to that of CTRL mice and indicated higher freezing behavior than CKO mice (CTRL n = 26, CKO n = 26, CTRL + PDE4B n = 10, CKO + PDE4B n = 11; CTRL vs. CKO, *p = 0.0348; CKO vs. CTRL + PDE4B, *p = 0.0355; CKO vs. CKO + PDE4B, ***p < 0.001; two-way ANOVA). Individual data points representing the number of animals or samples used are shown for all experiments. All samples were collected and experiments performed at ZT12. Data are represented as the mean ± SEM. N.S. denotes non-significant, *p < 0.05, **p < 0.01, and ***p < 0.001. Scale bars, 100 μm (B, 10×), 50 μm (top in D, 20×), and 2 μm (bottom in D, 63×, zoom 4.5).

KEY RESOURCES TABLE

REAGENT or RESOURCE	SOURCE	IDENTIFIER
Antibodies		
anti-TIMELESS	Abcam	Cat# ab72458; RRID:AB_1271226
anti-TIMELESS	Abcam	Cat# ab50943; RRID:AB_883003
anti-NeuN	Millipore	Cat# MAB377; RRID:AB_2298772
anti-CaMKIIα	Millipore	Cat# C265; RRID:AB_2067919
anti-GFAP	Thermofisher	Catalog # PA1–10004; RRID:AB_1074620
anti-PDE4B	Abcam	Catalog #ab170939; RRID:AB_2927553
anti-GluAI	Millipore	Cat# 04–855; RRID:AB_1977216
anti-GluA1-pSer845	Millipore	Cat# AB5849; RRID:AB_92079
anti-b-actin	Sigma Aldrich	Cat# A5316; RRID:AB_476743
Goat anti-Rabbit IgG (H+L) Secondary Antibody, Alexa Fluor® 488 conjugate	Thermofisher	Cat# A-11008; RRID:AB_143165
Goat anti-Mouse IgG (H+L) Cross-Adsorbed Secondary Antibody, Alexa Fluor 647	Thermofisher	Cat# A-21235; RRID:AB_2535804
Goat anti-Chicken IgY (H+L) Secondary Antibody, Alexa Fluor 647	Thermofisher	Cat# A-21449; RRID:AB_2535866
IRDye® 800CW Goat anti-Rabbit IgG (H + L) Secondary Antibody	Licor	Cat# 926–32211; RRID:AB_621843
IRDye® 680RD Goat anti-Mouse IgG Secondary Antibody	Licor	Cat# 925–68070; RRID:AB_2651128
Bacterial and virus strains		
AAV9- *CaMKIIα*.eGFP-CRE	Addgene	105551-AAV9
AAV-DJ(N589X).hSyn.mPDE4B.IRES. mCherry.WPRE.SV40	Penn Vector	Custom made
Chemicals, peptides, and recombinant proteins		
Tamoxifen	Sigma Aldrich	Cat# T5648
PBS (10X), pH 7.4	Thermofisher	Cat# 70011069
PFA 20% Solution	EMS	Cat# 100496–494
Tissue-Tek O.C.T. Compound, Electron Microscopy Sciences	VWR	Cat# 102094–104
Triton® X-100 Surfactant	Millipore Sigma	Cat# TX1568–1
Goat Serum (NGS)	Sigma Aldrich	Cat# G9023–10ML
Hydromount	National Diagnostics	Cat# HS-106
Protease Inhibitor Cocktail Set III, EDTA-Free	Millipore	Cat# 539134
Phosphatase Inhibitor Cocktail 2	Millipore	Cat# P5726
Pierce™ BCA Protein Assay Kit	Thermofisher	Cat# 23225
NuPAGE® LDS Sample Buffer (4X)	Thermofisher	Cat# NP0007
NuPAGE® Sample Reducing Agent (10X)	Thermofisher	Cat# NP0009
7.5% Mini-PROTEAN® TGX™ Precast Protein Gels, 12-well, 20 µl	BioRad	Cat# 4561025

REAGENT or RESOURCE	SOURCE	IDENTIFIER
Nitrocellulose/Filter Paper Sandwiches 0.2 um 7 × 8.5 cm	BioRad	Cat# 1620212
RNA extraction kit	Zymo	Cat# R2053
cDNA synthesis kit	Thermofisher	Cat# AB1453B
SsoAdvanced® Universal SYBR® Green Supermix	BioRad	Cat# 1725270
Picrotoxin	Millipore Sigma	Cat# P1675
NBQX	Cayman Chemical Co.	Cat# 14914
KCl	Sigma Aldrich	Cat# P3911
NaH_2PO_4	Sigma Aldrich	Cat# S9638
CaCl2	Sigma Aldrich	Cat# C8106
$MgCl_2$	Sigma Aldrich	Cat# M2670
$MgSO_4$	Sigma Aldrich	Cat# M1880
Glucose	Sigma Aldrich	Cat# G8270
NaCl	Sigma Aldrich	Cat# S7653
$NaHCO_3$	Sigma Aldrich	Cat# S6014
Cesium hydroxide	Sigma Aldrich	Cat# 23204
D-gluconic acid	Sigma Aldrich	Cat# G1951
EGTA	Sigma Aldrich	Cat# E4378
HEPES	Sigma Aldrich	Cat# H3375
KOH	EMD Millipore	Cat# 109108
NMDG	Sigma Aldrich	Cat# M2004
Sodium ascorbate	Sigma Aldrich	Cat# A4034
Thiourea	Sigma Aldrich	Cat# T8656
Sodium pyruvate	Sigma Aldrich	Cat# P2256
HCl	Fisher Chemical	Cat# SA49
Critical commercial assays		
EZ-ChIP Kit	Merck Millipore	Cat# 17–371
Magna ChIP™ G Tissue Kit	Merck Millipore	Cat# 17–20000
Cyclic AMP Complete ELISA kit	ENZO Life Sciences	Cat# ADI-900–163
Deposited data		
ChIP-seq data (for Figures 4, S8 and Table S2)	This paper	GEO: GSE208149
Experimental models: Organisms/strains		
C57BL/6N-A<tm1Brd>Timeless<tm1a (EUCOMM) Hmgu>/Wtsi	EMMA	RRID: IMSR_EM:10347
B6;129S6-Tg (Camk2a-cre/ERT2)1Aibs/J	Jackson Labs	RRID: IMSR_JAX:012362
Oligonucleotides		
Quantitative RT-PCR forward primer for *Timeless*: 5'-ATGAACTGTGAACTT CTAGCCAC-3'	This paper	N/A

REAGENT or RESOURCE	SOURCE	IDENTIFIER
Quantitative RT-PCR reverse primer for *Timeless*: 5'-CCTCAGGTATCGG ATCAAATCCT-3'	This paper	N/A
Quantitative RT-PCR forward primer for *Pde4b*: 5'-GCGAGATGGCTTCAA ACAA-3'	This paper	N/A
Quantitative RT-PCR reverse primer for *Pde4b*: 5'-CAGACACCTGGTTCC CTGAT-3'	This paper	N/A
Quantitative RT-PCR forward primer for *GluA1*: 5'-CTAGGCTGCCTGAAC CTTTG-3'	This paper	N/A
Quantitative RT-PCR reverse primer for *GluA1*: 5'-GGGAAGATTGAATGG AAGCA-3'	This paper	N/A
Quantitative RT-PCR forward primer for *β-Actin*: 5'-ATGGAGGGGAATAC AGCCC-3'	This paper	N/A
Quantitative RT-PCR reverse primer for *β-Actin*: 5'-TTCTTTGCAGCTCCT TCGTT-3'	This paper	N/A
Software and algorithms		
Matlab	MathWorks	https://www.mathworks.com/products/matlab.html?s_tid=hp_products_matlab MATLAB (RRID: SCR_001622)
Prism 9	GraphPad	https://www.graphpad.com/scientificsoftware/prism/ GraphPad Prism (RRID: SCR_002798)
IgorPro7	Wavemetrics	https://www.wavemetrics.com/ IGOR Pro (RRID: SCR_000325)
Origin Pro 9	Origin Lab	https://www.originlab.com/ Origin (RRID: SCR_014212)
Multiclamp 700B	Molecular Devices	https://www.moleculardevices.com MultiClamp 700B Microelectrode Amplifier (RRID: SCR_018455)
ImageJ	ImageJ	http://imagej.net/Welcome ImageJ (RRID: SCR_003070)
DiscoRhythm R package	DiscoRhythm 1.2.1	https://mcarlucci.shinyapps.io/discorhythm/